Cluster formation in fluids with competing short-range and long-range interactions

Martin B. Sweatman,[1]* Rui Fartaria[1] and Leo Lue[2]

[1]Institute of Materials and Processes, School of Engineering, University of Edinburgh, Edinburgh EH9 3JL, UK.

[2]Department of Chemical and Process Engineering, University of Strathclyde, Glasgow G1 1XJ, UK.

ABSTRACT

We investigate the low density behaviour of fluids that interact through a short-ranged attraction together with a long-ranged repulsion (SALR potential) by developing a molecular thermodynamic model. The SALR potential is a model of effective solute interactions where the solvent degrees of freedom are integrated-out. For this system, we find that clusters form for a range of interaction parameters where attractive and repulsive interactions nearly balance, similar to micelle formation in aqueous surfactant solutions. We focus on systems for which equilibrium behaviour and liquid-like clusters (i.e. droplets) are expected, and find in addition a novel coexistence between a low density cluster phase and a high density cluster phase within a very narrow range of parameters. Moreover, a simple formula for the average cluster size is developed. Based on this formula, we propose a non-classical crystal nucleation pathway whereby macroscopic crystals are formed via crystal nucleation within microscopic precursor droplets. We also perform large-scale Monte Carlo simulations, which demonstrate that the cluster fluid phase is thermodynamically stable for this system.

Keywords: Liquid mixtures, clustering, competing interactions, mesostructure, non-classical nucleation

1. Introduction

Clustering in fluids is important in many areas of science and engineering, such as in protein solutions[1], pharmaceutical crystallisation[2], biomineralisation[3], and nanotechnology[4-6]. For example, the aggregation of proteins influences their structure and function and is associated with specific diseases[7], including neurodegenerative diseases such as Alzheimer's. In addition, proteins are thought to form "rafts" in cell wall membranes[8-10]. Moreover, exploiting clustering and self-assembly of peptides or nanoparticles in solution is considered to be a useful method for the design and manufacture of novel nanomaterials, such as peptide-based bio-scaffolds[11] or novel sensors[12]. Naturally, understanding cluster formation is fundamentally interesting and important, but particular difficulties arise when the clustering particles, and perhaps even the clusters themselves, cannot be imaged directly *in-situ*. For these cases, statistical thermodynamic models of clustering take on increased importance.

Perhaps the simplest model that exhibits clustering is the "short-range attractive, long-range repulsive" (SALR) potential model. This one-component model of solute particles, where the solvent degrees of freedom have been integrated-out, involves only spherically-symmetric pair-interactions, and as such can be considered a "simple" fluid. That such a simple model can give rise to behaviour normally associated with more complex molecules, such as surfactants or block copolymers,

provides the impetus to understand its behaviour in more detail. A great deal of theoretical, simulation and experimental work has focused on SALR systems for which the range of the attractive interactions is short compared to the particle "core" diameter because this regime is considered to be relevant for protein solutions. Colloid-polymer mixtures with effectively similar interactions (where the polymer radius of gyration is small compared to the colloid diameter) are often studied to provide insight in this regime because the particles and/or clusters can be imaged directly[1]. For these systems, characterized by $\zeta \sim 0.1$, where ζ is the ratio of the range of the attraction to the size of the core, interesting behaviour arises when the strength of attractive interactions is several times $k_B T$, where k_B is the Boltzmann constant and T is the absolute temperature (let's call this energy-scale ratio ε). This behaviour is generally characterized by the formation of small clusters with intermediate-range order at low solute concentrations, which tend to elongate and form arrested networks and gels as the particle concentration is increased[1,13-22]. Similar arrested network formation is also observed in the absence of long-ranged repulsive interactions[23] (e.g., in "diffusion limited aggregation" and attractive glasses), and in the absence of short-ranged attractions[21] (e.g., in repulsive, or "Wigner", glasses). This non-equilibrium behaviour masks the underlying equilibrium structures that would result from competition between attraction and repulsion. Moreover, because the length scales, and hence time scales, are very different between colloidal and protein domains, it is not always clear whether the directly observed colloidal structures are generally representative of protein clusters. As such, the physics of equilibrium SALR structures is less well understood.

One important aspect of this physics involves so-called "two-step" crystal nucleation, whereby crystal nucleation occurs within a liquid-like cluster[24-27] (that is, the liquid cluster nucleates and forms first on short time-scales, followed by crystal nucleation within the cluster on longer time-scales). If the timescale for crystal nucleation is much longer than cluster formation this two-step process can only occur if microscopic liquid-like precursor solute clusters can be stabilized, and is another reason for the interest in SALR fluids. This two-step process is considered distinct from classical crystal nucleation where solute aggregation and crystal structure formation occur simultaneously, and is associated with diseases such as sickle-cell anemia[28,29]. It is also suggested to occur in some molecular mixtures such as glycine solutions[30,31], and so could be important for the design of continuous crystallization processes for pharmaceuticals[2]. Equilibrium SALR structures can be expected to arise naturally when $\zeta \sim 1$ and $\varepsilon \sim 1$, since for these systems local re-ordering can easily occur. Unfortunately, there is no experimental work in this region of the phase diagram with colloid-polymer mixtures, and consequently our understanding of equilibrium clustering and two-step nucleation of the SALR model is incomplete. However, the recent work of Bartlett and co-workers[32,33] with uncharged colloid-polymer mixtures with $\zeta \sim 1$ suggests that such experiments might be feasible.

Many approaches have been used to examine equilibrium SALR systems, from Monte-Carlo simulation[34] through to thermodynamically consistent integral equation approaches[20] and density functional theories[35], yielding insight into specific systems such as clustering in 2-dimensional films[36] and the 3-dimensional SALR system considered in this work[37]. A good introduction of this body of work is provided by Wilding and Archer[34]. While much has been learned about fluid structure and thermodynamics at intermediate densities, both for disordered cluster fluid states and ordered, or "modulated", cluster phases at intermediate density[34,35,37-39], the low density cluster fluid phase is much less well studied. To be clear, we define a disordered cluster fluid phase as one that is

isotropic, but actually consists of a uniform dispersion of large clusters of particles. The aim of this work is to better understand this low density part of the equilibrium SALR phase diagram.

For these SALR systems, the Lifshitz point and lambda-line are sometimes analyzed[37,40,41], which often involves locating mechanical instabilities in the uniform fluid without clusters. However, these techniques are incapable of providing the precise location, or clarifying the nature, of associated phase transitions, which are of thermodynamic origin.

Monte Carlo simulations have revealed that for the equilibrium SALR fluids of interest here, $\zeta \sim 1$, a series of modulated phases with increasing density are expected[34], starting with an ordered phase of spherical clusters (a cluster solid), followed by columnar, lamellar, and ordered columnar and spherical bubble phases. All these phases occur at densities "intermediate" between the uniform vapour and liquid phases. The usual bulk vapour-liquid transition is metastable with respect to these modulated phases. However, Archer and Wilding[34] do not investigate the disordered cluster fluid phase at low density. They clearly do find states corresponding to a single spherical cluster with liquid-like density surrounded by a vapour, but due to the periodic boundary conditions they use, such isolated clusters correspond to an ordered cluster (simple cubic) solid phase, not a cluster fluid phase. On the other hand, molecular simulations[13-16] and experiments[17-19] in the region where $\zeta \sim 0.1$ demonstrate that small irregular clusters exist at low densities even if they are not always at equilibrium[42]. Our interest here is in understanding how this behaviour is changed for $\zeta \sim 1$, where equilibrium structures are expected.

Spatially ordered aggregates can also be modeled using standard density functional or self-consistent field-theoretic approaches[35,38,39]. However, the disordered cluster fluid phase we investigate here, consisting of a dispersion of liquid-like droplets, has so far avoided treatment using these methods. From a theoretical perspective, the likely reasons for this are that within this phase, the clusters themselves behave like mesoscopic fluid particles, and therefore there are strong, long-range correlations in the pair density. The usual mean-field approaches do not capture these long wavelength correlations and so do not exhibit the correct physics. For example, Jiang and Wu[43] attempt to investigate a cluster fluid at low density for a similar SALR potential to that investigated here using mean-field DFT. They find a non-uniform solution to their model, consisting of a spherical cluster at the origin surrounded by a uniform vapour, and identify this solution with the cluster fluid. They take this as an indication that the system will form an isotropic dispersion of clusters. This approach is similar to the earlier work for surfactant micelles by Stillinger[44] for aqueous surfactant systems. However, the difficulty with this interpretation is that the vapour surrounding the central cluster is "cluster-less", because the mean-field DFT they use does not describe a uniform dispersion of clusters. That is, it cannot generate the pair or higher body distribution functions of a cluster fluid. Note, the difference between an isotropic clustered and "un-clustered" fluid is not the equilibrium density profiles, which can be identical, but rather the *correlations* within the systems. This seems to indicate that conventional density functional theories do not properly account for the long range correlations that lead to the formation of these clusters.

Bomont et al.[20] use a thermodynamically self-consistent integral equation theory to analyze the onset of equilibrium clustering at intermediate densities in the approach to modulated phases, signified by mechanical instabilities (the lambda-line), in the $\zeta \sim 0.1$ regime of SALR fluids. The advantage of this approach, compared to other integral equations, is illustrated further by Bomont and colleagues[41,45] and Kim et al.[46], who are able to find solutions to their integral equations in regions of parameter-space at intermediate densities where most other approximate integral

equations fail. Indeed, Bomont et al. find intriguing jumps[45] in the first peak of the radial distribution function for a range of SALR parameters similar to those used here, indicative of a potential phase transition from a uniform phase of clusters to a non-uniform (modulated) clustered phase at intermediate densities. Despite the significant advance this approach brings, the nature of this phase transition is not clear and no results are provided at low density. We return to this work in our summary, and re-interpret their results in light of our findings.

From a simulation perspective these phases are difficult to treat due to their size (because of the longer range of the interactions when $\zeta \sim 1$, compared to $\zeta \sim 0.1$, each cluster can involve hundreds to thousands of particles, and many clusters need to be simulated for a cluster fluid), the existence of long-range interactions which requires lengthy summations over particle pairs, and poor sampling of configurations unless advanced cluster-move algorithms are used that treat separately the length-scales involved. These considerations, when combined, lead to expensive simulations.

Interestingly, a straightforward treatment of the low density SALR cluster fluid is achieved through a kind of micelle theory[47-51]. Groenewold and Kegel[52] applied this kind of method to colloidal dispersions modeled with a more sophisticated variant of the SALR model. Their model includes the effect of charge binding at a colloid surface, and so the long-range screened-coulomb repulsion is generated in a more self-consistent manner. Their main result concerns the charge of a colloidal cluster, and they do not consider phase behaviour more generally. Later, Foret and Destainville[53] applied this kind of approach directly to an SALR fluid, focusing on a region of the phase diagram analogous to pre-micellization. However, despite this earlier work, the wider phase behaviour of the equilibrium SALR fluid at low density remains unexplored.

In summary, the modulated, or ordered, equilibrium phase behaviour of SALR fluids at intermediate density is well studied, but little progress has been made with the disordered cluster fluid phase at low density for $\zeta \sim 1$. In the next section, we develop a molecular thermodynamic model that goes beyond the mean-field level and is able to describe this disordered cluster fluid phase. We then relate this model to theories for micelle formation in surfactant solutions. In section 3, we apply this thermodynamic model to examine the low density phase behaviour of these SALR systems. In brief, for the same 3-dimensional SALR system studied by Archer et al.[37], we find micelle-like behaviour at low density and identify a critical cluster concentration. We expect that transitions from the cluster fluid phase to ordered (modulated) phases occur at higher densities. Interestingly, we locate a novel cluster-vapour to cluster-liquid phase transition over a very narrow range of SALR parameters with weaker attractive interactions. We also remark on a potential mechanism for two-step non-classical crystal nucleation. In section 4, we compare results of the thermodynamic model with large-scale Monte Carlo simulations at a single state point, and conclude with a summary of this work in section 5.

2. Theory

2.1 SALR fluid model

The system of interest in this work comprises spherical particles interacting through a core of diameter *d* (taken to be a hard sphere here) plus a short-range attraction and a longer-ranged repulsion (the SALR potential),

$$\phi(x) = \phi_{HS}(x) + \phi_{SALR}(x) \qquad (1)$$

where $x = r/d$ and r is the separation between a pair of particles. A convenient form of the SALR potential is provided by the combination of two Yukawa potentials for $x > 1$,

$$\beta\phi_{SALR}(x) = -\frac{A_a}{x}\exp(-z_a(x-1)) + \frac{A_r}{x}\exp(-z_r(x-1)) \qquad (2)$$

where $\beta = 1/(k_BT)$. The parameters A_a and A_r(both > 0) determine the strength of attractive and repulsive interactions, respectively, relative to k_BT, while the parameters z_a and z_r (with $z_a > z_r$) determine their range. So, four independent parameters are needed to define the SALR model, including temperature. A fifth independent parameter is the overall system density, ρ_b. The SALR potential for a set of parameters investigated in this work (A_a= 2.0, A_r= 0.5, z_a = 1.0, z_r = 0.5) is shown in Figure 1a. The choice z_a = 1.0 should result in equilibrium clusters rather than non-equilibrium arrested states.

In this work, **we fix A_r = 0.5, z_a = 1.0, and z_r = 0.5, and consider the effect of varying A_a.** In experiments with colloid-polymer mixtures, this choice corresponds to keeping the temperature, colloid charge and solvent dielectric constant fixed (thus fixing A_r and z_r), and varying the concentration (but not the radius of gyration) of polymer such that the depletion potential strength (but not range) induced by the polymer is varied. For other experimental systems this set of parameters will correspond to other experimental constraints, and possibly involve manipulating the temperature. For example, for modeling mesostructure in liquid mixtures the long-ranged repulsive term would correspond to a model of the screened coulomb interaction between solutes caused by charge dissociation of the solute in the solvent, while the short-ranged attractive term might correspond to hydrogen bonding or other short-ranged dispersive interactions between solute molecules.

2.2 Thermodynamic model

We take an approach originally inspired by earlier work by one of us[54,55] concerning a coarse-grained density functional theory of adsorption. Our approach might also be called a 'minimal' or an 'order parameter' model[37]. Ultimately, we find that our molecular thermodynamic model resembles earlier models of micellization[47-51] in some respects.

We assume the disordered cluster fluid phase is composed of spherical clusters of particles (liquid-like droplets) with body-density $\rho_l = n_l/V_c$ and cluster density $\rho_c = n_c/V$ dispersed in a vapour of density ρ_v (here, n_l is the average number of particles per cluster of volume V_c, n_c is the average number of clusters in system volume V, and ρ_v is the average density of particles in the vapour outside the clusters). Actually, the system is not phase separated into vapour and liquid droplets *per se*; more properly, the vapour and clusters are all part of the same phase and cannot be treated separately. In general clusters are polydisperse in their size and shape. However, on average they are statistically identical, and so we choose them to be spherical and monodisperse, with diameter $d_c = 2R_c$; therefore, the density profile $P_c(\mathbf{r}-\mathbf{R})$ of a cluster centered at position $\mathbf{R}$ is

$$P_c(\mathbf{r}-\mathbf{R}) = \rho_l\Theta(R_c - |\mathbf{r}-\mathbf{R}|) \qquad (3)$$

where Θ is the Heaviside step-function. We show later that the polydispersity of the clusters is not expected to be very great for our model, and hence we are justified in neglecting fluctuations in size and shape polydispersity at this stage. We also assume for convenience a discontinuous, or sharp,

interface between the clusters and the background vapour, although this is not an essential feature of the model. The volume fraction φ of the clusters is

$$\varphi = \rho_c V_c = \frac{\rho_b - \rho_v}{\rho_l} \quad (4),$$

where $V_c=\pi d_c^3/6$ is the cluster volume.

We begin the development of the molecular thermodynamic model by partitioning the configurational Helmholtz free energy density f_c of the cluster fluid phase into energetic and entropic contributions

$$f_c = u_c - Ts_c = (u_{self} + u_{cc} + u_{cg} + u_{gg}) - T(s_{self} + s_{mix}) \quad (5)$$

where u_{self} and s_{self} are the internal, or self, energy and entropy densities of a cluster, u_{cc}, u_{cg} and u_{gg} are the energy densities arising from cluster-cluster, gas-cluster and gas-gas interactions, and s_{mix} is the entropy density of mixing of clusters and gas. In turn, to parallel the development of micellar theories, we group these energy and entropy contributions into two free energy contributions,

$$f = (u_{self} - Ts_{self}) + (u_{cc} + u_{cg} + u_{gg} - Ts_{mix}) = f_{self} + f_{mix} \quad (6)$$

namely f_{self}, which describes the free energy density of particles within the clusters, and f_{mix}, which is the mixing free energy density of gas particles and clusters. In the following, we develop simple expressions for f_{self} and f_{mix} in terms of the model parameters, ρ_b, ρ_v, ρ_l and ρ_c.

Self-free energy

The self-free energy of the clusters is composed of two terms

$$f_{self} = \rho_c(U_{self} - TS_{self}) \quad (7)$$

where U_{self} is the interaction energy between particles in a cluster, i.e. its self-energy, and S_{self} is the entropy of the particles within a cluster. To estimate U_{self}, we assume that the correlations between particles within a cluster are similar to those within a bulk liquid. Taking a "simple liquid" view, we choose a hard sphere fluid as reference, and so the interaction energy of particles within a cluster is given by

$$\begin{aligned} U_{self} &= \frac{1}{2}\int d\mathbf{r}d\mathbf{r}'\phi_{SALR}(|\mathbf{r}-\mathbf{r}'|;d)g_{HS}(|\mathbf{r}-\mathbf{r}'|;d,\rho_l)\int d\mathbf{R}\,P_c(\mathbf{r}-\mathbf{R})P_c(\mathbf{r}'-\mathbf{R}) \\ &= 2\pi\int dr\, r^2\phi_{SALR}(r;d)g_{HS}(r;d,\rho_l)P_{dc}(r) \end{aligned} \quad (8)$$

where $g_{HS}(r;d,\rho)$ is the bulk hard sphere radial distribution function for hard spheres of diameter d at density ρ, which we approximate using the Percus-Yevick (PY) theory[56], and $P_{dc}(r)$ is related to the form factor of the clusters and represents the geometric convolution of two cluster density distributions.

The self-entropy can be written in terms of the cluster density as

$$S_{self} = V_c s_v(\rho_l) + A_c s_A(\rho_l, \rho_v, d_c) \qquad (9)$$

In the first term on the left hand side s_v is the entropy density of a uniform liquid at the same average density as the cluster, while in the second term s_A is the entropic contribution per cluster of the cluster-gas interface. Here, we omit higher order contributions to the cluster entropy caused by fluctuations in the size of the cluster. This is discussed in more detail later, and we will see that cluster size fluctuations are not very large for the system under consideration here.

For the first term we once again take a simple liquid view and set

$$s_V(\rho_l) = s_{HS}(\rho_l, d) \qquad (10)$$

where $s_{HS}(\rho_l, d)$ is the entropy density of a hard sphere fluid with particle diameter d at the same fluid density. In this work we neglect the interfacial entropy per cluster, S_A, for convenience.

Mixing free energy

We deal with the contribution of the configurational energy density contribution to the mixing free energy first, which is given exactly by the usual energy equation[56],

$$\begin{aligned} u_{mix} &= \frac{\rho_b^2}{2V}\int d\mathbf{r}d\mathbf{r}'\phi_{SALR}(|\mathbf{r}-\mathbf{r}'|)g(|\mathbf{r}-\mathbf{r}'|) \\ &= \frac{\rho_v^2}{2V}\int d\mathbf{r}d\mathbf{r}'\phi_{SALR}(|\mathbf{r}-\mathbf{r}'|)g_{vv}(|\mathbf{r}-\mathbf{r}'|) \\ &\quad + \frac{\rho_v\rho_c}{V}\int d\mathbf{r}d\mathbf{r}'\phi_{SALR}(|\mathbf{r}-\mathbf{r}'|)\int d\mathbf{R}\,P_c(\mathbf{r}'-\mathbf{R})g_{vc}(|\mathbf{r}-\mathbf{R}|) \\ &\quad + \frac{\rho_c^2}{2V}\int d\mathbf{r}d\mathbf{r}'\phi_{SALR}(|\mathbf{r}-\mathbf{r}'|)\int d\mathbf{R}d\mathbf{R}'\,P_c(\mathbf{r}-\mathbf{R})g_{cc}(|\mathbf{R}-\mathbf{R}'|)P_c(\mathbf{r}'-\mathbf{R}') \end{aligned} \qquad (11)$$

where $g_{vv}(r)$ is the radial distribution function (rdf) between particles in the vapour, $g_{vc}(r)$ is the rdf between particles in the vapour phase and cluster centers, and $g_{cc}(r)$ is the cluster center-cluster center rdf. We now describe our approximations for these rdfs.

First consider taking the "simple fluid" view that locally fluid structure can be well approximated by a hard sphere reference fluid, in this case an additive hard sphere mixture of large spheres (representing clusters) and small spheres (representing particles in the gas). Unfortunately, this will not be accurate because it ignores effective interactions in the system. The effective interaction between two non-overlapping clusters whose centers are separated by $r=|\mathbf{R}-\mathbf{R}'|$ is

$$U_{cc}^{eff}(|\mathbf{R}-\mathbf{R}'|) = \int d\mathbf{r}d\mathbf{r}'\,P(\mathbf{r}-\mathbf{R})\phi_{SALR}(\mathbf{r}-\mathbf{r}')P(\mathbf{r}'-\mathbf{R}') \qquad (12)$$

A typical form of this effective cluster–cluster interaction is plotted in Figure 1b, along with its corresponding Mayer function. It shows that typical clusters experience a strong mutual repulsion at a range much larger than d_c, and hence do not approach each other closely. The effective interaction between a vapour particle and a cluster separated by r is

$$U_{vc}^{eff}(|\mathbf{R}-\mathbf{R}'|) = \int d\mathbf{r}' \phi_{SALR}(\mathbf{R}-\mathbf{r}') P(\mathbf{r}'-\mathbf{R}') \qquad (13)$$

A typical form of this effective vapour–cluster interaction is plotted in Figure 1c, along with its corresponding Mayer function. It shows that gas particles experience a weak repulsion around clusters at a range somewhat larger than d_c, but much less than the range at which clusters experience a strong mutual repulsion. Consequently, if we are to represent the system in terms of a hard sphere mixture, this system corresponds approximately to a highly size-asymmetric hard sphere mixture with significant negative non-additivity. For the case shown in Figures 1b and 1c the non-additivity parameter would be Δ ~-0.5. Unfortunately, there are no robust analytical theories for the radial distribution functions of such systems in the literature. We proceed by making the following approximations for the rdfs,

$$\begin{aligned}
g_{cc}(r) &= \begin{cases} \exp(-\beta U_{cc}^{eff}(r)) & ; \quad r > r_{cc}^{\min} \\ 0 & ; \quad r < r_{cc}^{\min} \end{cases} \\
g_{vc}(r) &= \begin{cases} g_{vc}^{mix}(r;\rho_v,d,\rho_c,d_c)\exp(-\beta U_{vc}^{eff}(r)) & ; \quad r > r_{vc}^{\min} \\ g_{vc}^{mix}(r;\rho_v,d,\rho_c,d_c)\exp(-\beta U_{vc}^{eff}(r_{vc}^{\min})) & ; \quad r < r_{vc}^{\min} \end{cases} \\
g_{vv}(r) &= g_{vv}^{mix}(r;\rho_v,d,\rho_c,d_c)
\end{aligned} \qquad (14)$$

where $g_{xx}^{mix}(r;\rho_1,d_1,\rho_2,d_2)$ are the rdf components of an additive binary hard sphere mixture (which we approximate in terms of the PY functions obtained from a Fundamental Measure Theory[55]) with component densities ρ_1 and ρ_2 and component diameters d_1 and d_2 respectively, and $r_{xx}^{\min}$ are the separations corresponding to the minima of $\exp(-\beta U_{xx}^{eff}(r))$.

Note that the model for the energy density is multi-scale in the sense that it simultaneously includes radial distribution functions on primary particle and cluster length-scales, with the cluster-cluster and gas-cluster rdfs determined through equations (19) to (21) where equations (19) and (20) also incorporate these multiple scales.

For a uniform fluid without clusters we have

$$u = 2\pi\rho_b^2 \int_0^\infty dr r^2 \phi_{SALR}(r) g_{HS}(r;d,\rho_b) \qquad (15)$$

We now deal with the mixing entropy of the system; this is where we introduce the key ingredient that generates a non-mean-field theory similar to theories of micellization. The entropy of mixing accounts or the entropy of the coarse-grained system

$$s_{mix} = s_{HS}^{-mix}(d,\rho_v,d_c,\rho_c,d_c^{eff}) + \rho_c S_{com} \qquad (16)$$

The first term on the left-hand side approximates this entropy in terms of an asymmetric binary hard sphere mixture with significant negative non-additivity, where the clusters are treated as large spheres with diameter d_c, and the primary particles are treated as small spheres with diameter d, but the cluster-cluster effective interaction corresponds to an effective diameter d_c^{eff}. We approximate this effective diameter in terms of the Barker-Henderson prescription[56]

$$d_c^{eff} = \int_0^\infty dr\,(1-\exp(-\beta U_{cc}^{eff}(r)) \qquad (17)$$

The second term in (16) is a center of mass correction, which ensures the coarse-grained clusters have a precisely defined position, and is described later.

Clearly, this approximation for s_{mix} does not take into account the effect of U_{vc}^{eff} on the distribution of primary particles surrounding each cluster. Nor does it take into account the effect of the direct interaction between primary particles in the vapour on the mixing entropy. Nevertheless, it will be accurate for a dilute system with low vapour and cluster densities and is a convenient approximation at this stage. However, we are not aware of any well-tested thermodynamic theories for the entropy of such a hard sphere mixture, and so must develop our own prescription here. Fortunately, for this particular SALR system a very straightforward and convenient approximation can be found.

For this particular kind of hard sphere mixture consider the density profile of small particles surrounding the large particles. Provided this density profile is unaffected by most typical large particle configurations, then to a good approximation this system can be de-coupled and its entropy written accurately as

$$s_{HS}^{mix}(d,\rho_v,d_c,\rho_c,d_c^{eff}) = \xi s_{HS}(d,\rho_g) + s_{HS}(d_c^{eff},\rho_c) \qquad (18)$$

where $\rho_g = \rho_v/\xi$ is the vapour density between clusters, and $\xi = 1 - \varphi$ is the volume fraction of vapour. This approximation becomes more accurate as the size asymmetry and negative non-additivity increase. Once again, this approximation omits the contribution to the entropy of the primary particles due to their interface with the clusters. Because the cluster volume fraction ($\eta = \pi\rho_c d_c^3/6$) is typically quite low (< 0.1), this interfacial entropic contribution should be quite small.

Each hard sphere entropy term includes an ideal gas contribution and an excess hard sphere term,

$$-Ts_{HS}(d,\rho) = f_{id}(\rho) + f_{HS}^{ex}(d,\rho) = k_B T\rho(\ln(\rho)-1) + f_{HS}^{PYex}(d,\rho) \qquad (19)$$

Note that we have omitted terms in the ideal gas free energy density involving the thermal de Broglie wavelength of the primary particles, which are not required for this study on equilibrium phase behaviour. For the excess hard sphere free energy density, we use the PY compressibility result[56], which is quite accurate for packing fractions, $\eta = \pi\rho d^3/6$, up to the hard sphere freezing transition

$$\beta f_{HS}^{PYex}(d,\rho)/\rho = -\ln(1-\eta) + \frac{3\eta(1-\eta/2)}{(1-\eta)^2} \qquad (20)$$

The center of mass correction, S_{com}, arises because the coarse-grained clusters are required to have a well-defined position so that the entropy of mixing of the cluster and vapour can be evaluated. We define the cluster position by its center of mass. However, the cluster self-entropy density defined so far through equation (10) does not have a constrained center of mass; equation (10) simply refers to an equation of state for a bulk hard sphere fluid. Therefore, the cluster self-entropy density must be corrected to take account of this center of mass constraint. The effect of this

constraint on the cluster self-entropy can be estimated by considering how the position (i.e. the center of mass) of a cluster with *M* particles can be constrained to coincide with a specified cluster center position **s**. To achieve this, we can consider constraining the position of one of the particles in a cluster such that it counter-balances the positions of the other *M*-1 particles in the cluster to produce a center of mass at **s**. However, we must remember that this particular particle must remain part of the cluster as defined by the operational definition. Therefore its position is constrained to lie within a region V_c, the volume of the cluster, in order for it be counted as part of the cluster. Hence, the free energy of the system is increased by a factor approximately equal to

$$-k_B T \ln\left(P_{com}/V_c\right) \qquad (21)$$

per cluster, where P_{com} is the probability that the sum of the positions of the other *M*-1 particles (with respect to **s**) lies within a region such that it can be counter-balanced by the final particle, which is constrained to lie within V_c. The factor V_c in equation (21) arises because the position of this last particle is no longer free within V_c, but is instead constrained such that it counter-balances the cluster at **s**. Hence the configurational phase space available to the cluster is reduced by a factor of V_c. To make analytical progress, we make the simplification that V_c to be spherical (i.e. all particles within the cluster lie within a spherical region of radius $R_c = \sqrt[3]{3V_c/4\pi}$ centered at **s**) and take the case of an ideal gas. For this spherical ideal gas case the probability distribution function for the sum of positions, relative to **s**, of the *M*-1 particles corresponds to a random walk in 3-dimensional space of random step length less than R_c, and is given simply by IFT[$(\Theta(k;R_c)/V_c)^{M-1}$], where $\Theta(k;R_c)$ is the 3-D Fourier transform of the Heaviside step-function of radius R_c. The probability this lies within a region of radius R_c is

$$P_{com} = 4\pi \int_0^{R_c} dr r^2 IFT[\left(\Theta(k;R_c)/V_c\right)^{M-1}] \qquad (22)$$

We now seek an analytic approximation to this. For large *M* this distribution function in *k*-space is concentrated around *k* = 0. By expanding the *k*-space function around *k* = 0 in a Taylor series

$$\Theta(k;R_c)/V_c \approx 1 - \frac{k^2 R_g^2}{6} + \cdots \qquad (23)$$

where R_g is the radius of gyration of the cluster, we obtain

$$P_{com} \approx 4\pi \int_0^{R_c} dr r^2 IFT[\exp(-(M-1)(kR_g)^2/6)] \qquad (24)$$

Evaluating the 3D-Inverse Fourier transform gives

$$P_{com} \approx 4\pi \int_0^{R_c} dr r^2 \left(\frac{1}{2\sqrt{a\pi}}\right)^3 \exp(-r^2/4a) \qquad (25)$$

where $a = R_g^2(M-1)/6$. Integration gives

$$P_{com} \approx \frac{1}{6}\sqrt{\frac{1000}{\pi(M-1)^3}} \qquad (26)$$

The resulting approximation for the center of mass correction is then

$$S_{com} \approx k_B \ln \frac{P_{com}}{V_c} = k_B \ln\left(\frac{\rho_l}{6M}\sqrt{\frac{1000}{\pi(M-1)^3}}\right) \qquad (27)$$

Note that in the limit of diverging cluster size $\rho_c S_{com}$ vanishes.

For the uniform fluid of density ρ_b without clusters to be consistent with the above approximations for the cluster fluid we model the entropy density as

$$s = s_{HS}(d, \rho_b) \qquad (28)$$

Model summary

Our final expression for the configurational Helmholtz free energy density for the cluster phase is

$$\begin{aligned} f_c &= u_c - Ts_c = f_{self} + f_{mix} \\ &\approx \int d\mathbf{r}'\phi_{SALR}(|\mathbf{r}-\mathbf{r}'|;d)\frac{\rho_c}{2}g_{HS}(|\mathbf{r}-\mathbf{r}'|;d,\rho_l)\int d\mathbf{R}\,P_c(\mathbf{r}-\mathbf{R})P_c(\mathbf{r}'-\mathbf{R}) - T\varphi s_{HS}(d,\rho_l) + k_BT\rho_c \ln\left(\frac{6M}{\rho_l}\sqrt{\frac{\pi(M-1)^3}{1000}}\right) \\ &+ \int d\mathbf{r}'\phi_{SALR}(|\mathbf{r}-\mathbf{r}'|)\sum_{ij}\frac{\rho_i\rho_j}{2}\int d\mathbf{R}d\mathbf{R}'\,P_i(\mathbf{r}-\mathbf{R})g_{ij}(|\mathbf{R}-\mathbf{R}'|)P_j(\mathbf{r}'-\mathbf{R}') - T\left(s_{HS}(d_c^{eff},\rho_c) + \xi s_{HS}(d,\rho_g)\right) \end{aligned} \qquad (29)$$

where *i,j* stand for cluster (c) or vapour (v), $P_v(r) = \delta(r)$, and $M = \rho_l\pi d_c^3/6$ is the average number of particles per cluster. Note that the logarithmic terms involved in the centre of mass constraint ($\ln(P_{com}/V_c)$) and the ideal gas free energy of clusters ($\ln(\rho_c)$) can be combined to produce a dimensionless argument.

For a uniform phase without clusters this becomes

$$f(\rho_b) = 2\pi\rho_b^2\int_0^\infty dr r^2\phi_{SALR}(r;d)g_{HS}(r;d,\rho_b) - Ts_{HS}(d,\rho_b) \qquad (30)$$

For a uniform bulk liquid phase this approximation is reasonable provided the range over which ϕ^{SALR} varies is large compared to typical nearest neighbor separations, i.e. the liquid behaves like a simple liquid. Accordingly, we only consider an SALR fluid with relatively long-ranged interactions. For a uniform bulk vapour phase this approximation becomes increasingly accurate with reducing density, where the entropy dominates.

A system separated into bulk liquid and vapour phases has free energy density

$$f(\rho_b) = \varphi f(\rho_l) + \xi f(\rho_g) \qquad (31)$$

The free energy density of the cluster phase (equation (29)) correctly tends to this limit for very large clusters where $\rho_c \to 0$.

2.3 Solving the model

We wish to find the minimum of this free energy model with respect to the primary variables; ρ_v, ρ_l, ρ_c, at fixed overall density ρ_b. Accordingly, we set

$$\left(\frac{\partial f}{\partial x}\right)_{\rho_b} = 0 \qquad (32)$$

for each primary variable $x = \rho_g$, ρ_l, and ρ_c. These equations can be solved using a Newton-Raphson method where the differential terms are approximated by central finite differences.

We also apply physically reasonable constraints to the solution space as follows; the cluster volume fraction, φ, is constrained to be less than the hard sphere fluid volume fraction at fluid-solid coexistence, i.e. $\varphi < 0.496$; and the number of particles in a cluster, M, is constrained to be at least 2.0, as a cluster cannot be defined for fewer particles.

3. Results

We study the same 3-dimensional SALR fluid studied earlier by Archer and co-workers[37]. This will allow us to compare our results with theirs. Specifically, we set A_r= 0.5, z_a= 1.0, and z_r= 0.5. Results are obtained for a uniform fluid and the disordered cluster fluid using equations (29) and (30) for the configurational Helmholtz free energy density for a range of bulk densities, ρ_b, and values of A_a. The Newton-Raphson method is used to minimize the free energy density of the cluster fluid phase. The configurational chemical potential, μ, and pressure, P, are obtained by (central) finite differences using the standard thermodynamic relations $\mu = \mathrm{d}f/\mathrm{d}\rho_b$ and $P = \rho_b\mu - f$. For a given chemical potential, where two or more phases exist the equilibrium phase is the one with the highest pressure; the other phases are metastable.

3.1 The cluster fluid phase diagram

Figure 2 shows the phase diagram generated by this model at low densities, ρ_b< 0.1. We find that the cluster fluid forms for 1.55 <A_a< 2.51 when ρ_b< 0.1. This parameter range corresponds well with those where modulated phases are predicted to form at higher densities for this system, according to mean field DFT methods[37]. We will now discuss the features of this diagram. **All parameters are expressed in their reduced form, with an energy scale of β and length scale of *d*.**

Micelle-like behaviour

Figure 2 shows the cluster fluid phase separated from the uniform vapour (with pre-clusters) by the critical cluster concentration (black solid line). This is typical behaviour for micellar solutions. To explain this behaviour we choose initially to examine results at A_a = 2.0. Figure 3a shows how the free energy density of the cluster fluid phase varies with cluster density for three bulk densities close to the CCC. Here, the cluster fluid free energy density is minimized with respect to the liquid and vapour densities. When the bulk density is below the CCC the free energy minimum occurs when the

cluster density is nearly zero (corresponding to a bulk vapour with pre-clusters, i.e. the uniform fluid without clusters is always unstable relative to the cluster fluid or uniform vapour with pre-clusters). Above the CCC, the free energy minimum shifts to much larger cluster densities. To understand this behaviour we analyze (29) in terms of micelle theory[49]. First we re-write the free energy function in terms of the vapour and cluster densities as

$$\beta f_c(\rho_v,\rho_c) = \rho_v(\ln(\rho_v)-1) + \rho_c(\ln(L^3\rho_c)-1) + \beta f_{self}(\rho_c) + \beta f_{mix}^{ex}(\rho_v,\rho_c) \quad (33)$$

where the first two terms on the right are the ideal gas free energy density of the vapour – cluster mixture, the third term is the self-free energy density of clusters and final term accounts for the remaining "excess" mixing free energy density. Note there are several novel features in this expression. First, micelle theories typically set the excess mixing free energy density to zero and consider clusters of all sizes. Here, instead, we include approximations for both the configurational energy and entropy in the excess mixing free energy, but neglect fluctuations in cluster size. Second, theories of micellization typically set $L = d$ arbitrarily, whereas we find that $L^3 = V_c/P_{com}$ (i.e. the length-scale L) arises as a consequence of the cluster center of mass constraint, S_{com}. Finally, this derived expression contains no adjustable parameters. In contrast, micelle theories usually contain adjustable parameters that are calibrated to reproduce experimental data.

The vapour and cluster densities are linked through

$$\rho_b = \rho_v + M\rho_c \quad (34)$$

where $M = \rho_l V_c$, and V_c is given by (4). If we fix ρ_l and M equal to their values at the CCC, then we can simplify the analysis as follows. Minimizing (33) with respect to ρ_c gives

$$\rho_c = \rho_v^M \exp(-\beta\Delta G) \quad (35)$$

where ΔG is the driving force for aggregation

$$\Delta G = \left(\frac{\partial f_{self}}{\partial \rho_c}\right) + \left(\frac{\partial f_{mix}^{ex}}{\partial \rho_c}\right)_{\rho_v} - M\left(\frac{\partial f_{mix}^{ex}}{\partial \rho_v}\right)_{\rho_c} = \mu_{self} + \mu_{mix,c}^{ex}(\rho_v,\rho_c) - M\mu_{mix,v}^{ex}(\rho_v,\rho_c) \quad (36)$$

Note that μ_{self}, which is a constant now that ρ_l and M are fixed, includes a logarithmic term that balances dimensions in (35). If we specify the critical cluster concentration as the bulk density for which particles are divided equally between the vapour and clusters (i.e. when $\rho_v = M\rho_c$), then we find

$$\exp(-\beta\Delta G_{ccc}) = \frac{1}{M}\left(\frac{2}{\rho_{ccc}}\right)^{M-1} \quad (37)$$

which in turn leads to

$$\rho_c = \frac{\rho_v}{M}\left(\frac{2\rho_v}{\rho_{ccc}}\right)^{M-1} \exp(-\beta(\Delta G - \Delta G_{ccc})) \quad (38)$$

At low cluster and vapour densities, the excess mixture terms are insignificant, and we are left with

$$\rho_c = \frac{\rho_v}{M}\left(\frac{2\rho_v}{\rho_{ccc}}\right)^{M-1} \qquad (39)$$

This shows that below the CCC, when most particles are in the vapour, the cluster density grows geometrically with the vapour density as the CCC is approached with large exponent M-1. Close to and below the CCC, we can write this as

$$\rho_c \approx \frac{\rho_v}{M}\exp(-(M-1)(1-2\rho_v/\rho_{ccc})) \qquad (40)$$

which is observed as nearly exponential growth in the cluster density just below the CCC. However, above the CCC, nearly all the particles are within a cluster, and in this case we observe nearly linear growth

$$\rho_c \approx \frac{\rho_b}{M} \qquad (41)$$

These two very different growth regimes result in a sharp "knee" in the variation of cluster density with bulk density close to the CCC. We call clusters that form below the CCC 'pre-clusters' to distinguish these two very different regimes. This behaviour is illustrated in Figures 3b and 3c for A_a = 2.0. Figure 3b shows how the variation of cluster density with bulk density changes from being almost exponential below the CCC to almost linear just above the CCC. In experiments with micelle forming surfactants the CMC is often determined from plots of this kind by extrapolation of the linear trend above the CMC down to the abscissa. Figure 3c shows how cluster properties change in the vicinity of the CCC. Above the CCC they are nearly constant, while below the CCC they vary much more quickly, which provides further motivation for distinguishing clusters from pre-clusters. Experimental or simulation methods unable to resolve pre-clusters at the very low cluster concentrations in the exponential (or geometric) growth regime would erroneously conclude that this transition corresponds to a second order one, as suggested by Figure 3a. In fact, the free energy is continuous, except in the limit M ->∞, and as such the CCC is not a true phase transition (the CMC is sometimes referred to as a pseudo phase transition). Figure 2 shows that the CCC is less than the density of the bulk 'un-clustered' vapour-liquid binodal density, which is metastable, in this range of SALR parameters.

Figure 3d shows how the pressure of the bulk vapour and the cluster fluid vary with chemical potential. Below the CCC pre-clusters are very slightly more stable than a uniform vapour phase without any clusters. At the CCC, at ρ_b = 0.003155 in this case, the difference between the free energy of the uniform vapour without pre-clusters and the cluster fluid are indistinguishable on the scale of this plot because the cluster density is so low. Above the CCC the cluster fluid branch clearly separates from the uniform vapour phase. The cluster fluid chemical potential and pressure vary very slowly with bulk density, resulting in a highly compressible fluid.

Cluster size and a non-classical crystal nucleation pathway

Figure 4a shows how the cluster size varies with A_a and bulk density above the CCC. We see that the cluster size grows with increasing A_a, and it increases very slowly with increasing bulk density beyond the CCC. Figure 4b shows how the energy and entropy contributions to the free energy density vary with cluster size at A_a = 2.0 and ρ_b = 0.02, obtained by minimizing the free energy with respect to ρ_g and ρ_l at fixed ρ_b, holding d_c fixed at the given value. The cluster density is then given

via equation (4). Over this range of cluster sizes, which includes the minimum size at d_c= 13.5, the entropy and energy combine to produce a relatively flat free energy profile. Interestingly, the energy and entropy minima are located at almost precisely the same cluster diameter. This coincident behaviour is quite general for the cluster fluid phase and occurs because the energy and entropy densities are coupled through the background vapour density ρ_g, which is also minimized at the equilibrium cluster size. In essence, the cluster fluid energy density, which is dominated by the cluster self-energy, is minimized at the equilibrium cluster size. For larger or smaller clusters the cluster self-energy increases, increasing the chemical potential. Hence the background vapour density increases to match the chemical potential of particles in the cluster. In turn, the entropy density of the system is dominated by the vapour entropy, which produces a minimum coincident with its density minimum and the energy minimum.

Taking this analysis a step further, if the cluster self-energy is minimized at equilibrium, then taking the cluster volume fraction φ and body density ρ_l, as fixed, the cluster size can be determined from equation (8) by setting $\partial u_{self}/\partial d_c = 0$, which gives

$$\int_0^\infty dr r^2 \phi_{SALR}(r;d) g_{HS}(r;d,\rho_l) \frac{\partial \left(P_{dc}(r)/V_c \right)}{\partial d_c} = 0 \qquad (42)$$

Using equation (3) results in a relatively straightforward estimate for the equilibrium cluster diameter

$$\int_d^{d_c} dr\, r^3 \left(1 - \left(\frac{r}{d_c} \right)^2 \right) \phi_{SALR}(r;d) g^{(2)}(r;d,\rho_l) = 0 \qquad (43)$$

where we have replaced the approximate rdf used in the thermodynamic model, represented by the hard sphere function $g_{HS}(r;d,\rho_l)$, with the exact radial distribution function of the uniform liquid at the same body-density as the cluster, $g^{(2)}(r;d,\rho_l)$. This more general equation might find use in experiments, on colloidal dispersions for example, if the cluster diameter can be measured by an appropriate kind of microscopy for a range of experimental parameters, since then it might be possible to invert equation (43) to obtain the effective inter-particle interaction potential.

Figure 4c shows the predictions of this approximation against results for the full model. In each case we set $g^{(2)}(r;d,\rho_l) = g_{HS}(r;d,\rho_l)$ where ρ_l = 0.86, representing approximately the liquid density at A_a= 2.0. The agreement is quite satisfactory. Using equation (43), d_c is estimated to diverge at around A_a=2.51. However, for A_a greater than about 2.19 the cluster liquid density exceeds the hard sphere fluid freezing density and the Lennard-Jones fluid freezing density, which are both close to a reduced density ρ_b~ 0.935. Consequently, we expect clusters in the region A_a> 2.19 to be solid (indicated by a dotted line in Figure 2), and, therefore, for A_a> 2.19, the CCC would correspond to a bulk vapour - solid particle transition. To be clear, this is an estimate of the location of this transition, from liquid-like clusters to solid-like clusters. Its precise location is not important for this work, but if required could be evaluated by reformulating the model in terms of solid clusters, and comparing the resulting free energies with those of this fluid model.

Interestingly, equation (43) suggests that a change in the internal state of the clusters (i.e. from liquid to crystalline solid) along the CCC line at this point, which will be accompanied by a

discontinuous change in the radial distribution function, will likely result in a discontinuity in the cluster diameter. In turn this will result in a different estimate for the value of A_a at which the cluster size diverges, most likely lower than the present one. Indeed, given that the cluster size depends on the rdf through equation (43) it is conceivable that, for some systems, the cluster size can diverge at the point at which the clusters themselves solidify. This could have important consequences for crystal nucleation from solution of solutes that possess these kinds of effective SALR interactions. For example, one can imagine formation of a cluster fluid phase with liquid-like cluster droplets, a fast process, followed by a potentially slower process of droplet crystallization, which then in turn could prompt a divergence in crystal size towards formation of macroscopic crystal particles in solution. This proposed two-step nucleation process is very similar to that described by Vekilov and others[24-27]. It clearly derives from the two-step nucleation process described by ten Wolde and Frenkel[24], in the context of protein crystallization, concerning systems without long-range repulsions where critical fluctuations in a metastable fluid phase lead to an enhanced probability of crystal nucleation. In that particular work, the division in timescales between cluster formation and crystal nucleation within clusters, which has not been established here, is clear. An additional ingredient we add to the mechanism here concerns equation (43), which suggests the equilibrium crystal size can be different to the pre-cursor cluster size because of the change in rdf. Moreover, equation (43) suggests that if the effective interactions between solute particles can be adjusted (by adjusting pH or salt concentration for example) then nanocrystals of any desired size can be produced.

Divergence in cluster size

The Lifshitz point is defined to occur at the point where the uniform fluid becomes mechanically unstable with respect to density fluctuations with an infinite range. To locate the Lifshitz point, we use an approximation for the pair direct correlation function which is exact in the low density limit, i.e.

$$c^{(2)}(r,\rho_b) = \begin{cases} c_{HS}^{(2)}(r,\eta) & ; \quad r < d \\ \exp(-\beta\phi^{SALR}(r)) - 1 & ; \quad r \geq d \end{cases} \qquad (44)$$

Using equation (44) and finding the value of A_a or which $\rho_b c^{(2)}(k,\rho_b)_{k=0} = 1$ generates a Lifshitz point at A_a = 4.12 for the SALR potential used in this work. However, according to the model presented here and equation (43), the cluster diameter diverges when

$$\int_d^\infty dr \phi^{SALR}(r) g_d^{(2)}(r,\rho_l) r^3 = 0 \quad (45)$$

For the SALR model of this work equation (45) predicts a divergence in the equilibrium cluster size at A_a = 2.51, which is much less than for the Lifshitz point predicted earlier. However, as previously discussed, it is likely that clusters will solidify at A_a ~ 2.19, and so we suggest cluster size will actually diverge for 2.19 < A_a < 2.51.

Modulated phases

When the packing fraction of clusters reaches some upper limit we suggest a phase transition from a disordered cluster fluid phase to an ordered cluster solid occurs. If we consider clusters to behave as mesoscopic hard spheres with diameter d_c^{eff}, we can expect this transition to occur at the cluster packing fraction $\eta_c^{eff} = \pi\rho_c (d_c^{eff})^3 / 6 \sim 0.496$, equivalent to the hard sphere fluid packing fraction at

freezing. The locus of this transition line, from disordered to ordered cluster phase, is shown in Figure 2. We expect the modulated phases seen by Archer and Wilding[34] occur beyond this transition line.

Cluster vapour to cluster liquid transition

Over the narrow range $1.6<A_a<1.75$, the cluster fluid phase separates via a first-order transition into cluster vapour and cluster liquid phases for $\rho_b< 0.1$. Although the transition occurs over a narrow range of *bulk* vapour densities, the change in *cluster* density is proportionately much greater. The bulk density range over which the cluster vapour phase is stable is very narrow, and vanishes near to $A_a = 1.65$, resulting at higher values of A_a in a bulk vapour (with pre-clusters) to cluster *liquid* transition. We locate the phase transition densities by plotting μ against P and finding the intersection point of the cluster vapour and cluster liquid branches. Figure 5 shows one such plot for $A_a = 1.75$. A first-order phase transition is clearly visible. The cluster size is very similar in both the cluster vapour and liquid phases, changing from 10.66 to 10.81 at the transition at this value of A_a.

We suggest the mechanism for this transition is an effective depletion potential caused by effective vapour – cluster interactions. Consider again Figure 1c, which depicts this effective interaction for a typical set of SALR parameters. Although the thermodynamic model predicts the cluster vapour – cluster liquid transition occurs for smaller values of A_a than this, Figure 3c does give a good indication of strength and range of the effective vapour-cluster interaction. It will cause the vapour to be significantly depleted in the region surrounding each cluster. When two clusters approach each other these depletion zones overlap, causing the vapour density between the clusters to be suppressed further. So the net force of the vapour on each cluster results in a mutual cluster-cluster attraction along a vector joining cluster centers, characterized by a depletion potential. This potential will increase in magnitude as the vapour density increases (i.e. as A_a decreases – in agreement with Figure 2). Interestingly, this means that clusters experience two effective forces. First, they experience the direct effective cluster-cluster interaction, which is repulsive, given by equation (12) and illustrated in Figure 1b for the same SALR parameters. Second, there is the depletion potential mediated by the vapour, which is always attractive. These effective interactions compete on the length scale of clusters and beyond. So we have competing interactions over two different length scales. This suggests the possibility of a hierarchy of ordering over different length scales, i.e. the intriguing potential for clusters of clusters, or super-cluster phases. For much smaller clusters the depletion effect and size-asymmetry between clusters and primary particles will be proportionately smaller. For these reasons we expect this transition will vanish for much smaller clusters, typical of $\zeta \sim 0.1$.

The origin of this cluster vapour – cluster liquid transition in the thermodynamic model is the excess mixture free energy, $f_{mix}^{ex}(\rho_v, \rho_c)$. It has not been observed before in theoretical work because this term is normally ignored, i.e. set equal to zero, in micellization theories. Neither have previous simulations been large enough to observe it; a very expensive simulation consisting of perhaps several thousand clusters (i.e. several million particles) would be required. And, as explained earlier, experimental work has focused on the $\zeta \sim 0.1$ region of the phase diagram.

3.2 Fluid structure

The radial distribution function (rdf) features prominently in the energy density (see equations (8) and (11)). Figure 6 shows how the rdf predicted by the model changes with bulk density along an isotherm at $A_a = 2.0$ above the CCC, within the cluster fluid phase. The general shape of the rdf is similar to that predicted by self-consistent integral equation theories[20,41,45,46] and Monte Carlo

simulations[34]. The inset in Figure 6 shows the same results presented on a logarithmic scale. At higher densities, on approaching the suggested location of the transition to a modulated phase, we begin to see longer range structure on the scale of the cluster diameter develop, which is 13.5 at this temperature.

3.3 Cluster size distribution

Fluctuations in cluster size and shape around the equilibrium are expected, but the current model does not explicitly account for them. Nevertheless, it is useful to understand the expected extent of size and shape fluctuations in order to gauge their influence. In principle, this cannot be achieved precisely within the current model. However, the cluster size distribution can be estimated by minimizing the free energy density for a range of cluster sizes at fixed bulk density. Although this generates the free energy density for a cluster fluid with an average cluster size not equal to the equilibrium size, rather than for a system with fluctuations in the cluster size around the equilibrium, it should nevertheless provide a reasonable estimate of cluster size fluctuations provided the cluster density is very small, since then cluster – cluster interactions are insignificant and we can consider a cluster in isolation.

To this end we choose A_a = 2.0 and ρ_b = 0.01, which is somewhat above the CCC but with sufficiently low cluster effective packing fractions0.05 < η_c^{eff} < 0.074such that clusters are largely isolated. The relative probability of a fluctuation in the size of a single clusteris given bythe exponential of the free energy density of that state multiplied by the system volume per cluster, i.e.

$$P(d_c) \propto \exp(-\beta f_c(d_c)/\rho_c) \quad (46)$$

Figure 7 shows how this estimate for the relative probability varies with cluster diameter for the above cluster fluid phase. We see that d_c is expected to vary within the rather narrow range 13.5 ± 0.7 to 2 standard deviations. We consider this justifies the neglect of explicit cluster size and shape fluctuations within the model, which we expect will have a relatively small influence for this system. However, we should be aware that other types of SALR model with either different parameters or different forms of interaction potential might generate larger cluster size fluctuations.

4. Comparison with Monte Carlo simulations

Monte Carlo simulations were used to verify the model's predictions, specifically the existence of a cluster fluid and cluster characteristics such as cluster density and size. More detailed comparison of theory and simulation is left for another publication, including verification, or otherwise, of the cluster vapour to cluster liquid transition.

The SALR parameters used were A_a=2.0, A_r = 0.5, z_a = 1.0 and z_r = 0.5 and therefore a bulk density of 0.02, which we expect to correspond to the cluster fluid (see figure 2), was chosen. A total of 10648 particles were used. Simulating systems that have long-range interactions and structure on multiple scales presents several difficulties, which we now describe, together with the strategies adopted to overcome them. Very long range interactions demand a large cutoff in the interactions and expensive pairwise energy sums. In this case a cutoff of 15 times the hard sphere diameter was used together with standard cell lists[58]. To enable the sampling of both vapour and cluster internal structure by standard Monte Carlo moves a dual displacement size was employed with step sizes of 0.1 and 1.5 hard sphere diameters selected at random with probability 0.8 and 0.2, respectively. In

order to sample the cluster fluid phase efficiency, cluster moves[58] were also used. After a calibration process a bond length of 2.0 hard sphere diameters was chosen to define clusters within each microstate. This bond length allows the translation and rotation of clusters as a whole unit, together with a portion of the vapour phase that surrounds each cluster, and leads to efficient sampling. Much shorter or longer bond lengths were found to be less efficient.

An initial trial simulation was started from a fully dispersed state, allowed to evolve to form clusters, and then reach equilibrium. The result was the formation of a cluster phase of relatively small clusters, when compared to the predictions of the thermodynamic model. For sufficiently long simulations we expected to observe clear steps in the configurational energy, corresponding to the fusion or evapouration of these small clusters. However, it soon became apparent that this would be a very rare event and that in practice once a specific number of clusters is established, they remain stable. Essentially, each cluster state is metastable within this sampling scheme. This is a consequence of the strong repulsion between clusters at short range, which prevents fusion events, and the nature of the free energy dependence on cluster size, which tends to prevent cluster evapouration once clusters have achieved a sufficiently large size.

Therefore, another strategy was adopted. Our aim is to simulate several metastable cluster states where the number of large clusters is fixed to evaluate their energy. The thermodynamic model indicates that the free energy minimum coincides with the energy minimum. So, accepting this result, we can determine the equilibrium number of large clusters for our chosen number of particles and system volume (which are fixed) by finding which cluster state (i.e. the simulation with a given number of large clusters) with the lowest energy. Our simulation strategy to achieve this aim consists of three steps; i) establish initial conditions for several simulations with a given number of large clusters, ii) perform simulations to find the locally stable behaviour for each metastable state, iii) compare resulting energies to find the global equilibrium state (assuming, as revealed by the theory, that it is dominated by energy). It is important to note that we are not interested in evaporation, nucleation, splitting or merging of clusters, because this would change the number of clusters, which we want to remain fixed in each simulation. We wish only to sample microstates of metastable cluster states so that we can evaluate their respective energies . We proceeded as follows.

Starting from the initial simulation described earlier with a large number of clusters, new cluster states, with fewer, larger clusters, were generated by choosing the smallest clusters and dispersing them. To achieve this we generated a table of the cluster size distribution. The largest X clusters were allowed to remain (where X is the target number of large clusters for that simulation), but the remaining clusters larger than 50 particles in size were dispersed. Dispersion of these clusters occurred simply by assigning random positions to their particles. Note that the cluster size distribution for all simulations has a broad 'zero' in the region of 50 particles, which justifies our choice of this cluster size to distinguish between large stable clusters and small volatile clusters. The small volatile clusters, which generally consist of just a few particles, are able to nucleate and evapourate readily in each simulation, and so there is no need to disperse them. Once the desired number of large clusters is achieved each simulation is stable and *no further re-distribution of clusters is required*. Having achieved suitable initial conditions for each simulation, ensemble averages are calculated after further equilibration. The straightforward cluster moves and dual-step-size sampling we use are sufficient for this purpose. Within these metastable cluster simulations clusters are relatively mobile, remain apart from each other and interchange particles through the background vapour (a movie[59] of the simulation with 13 large clusters is available as supplementary

material at [URL will be inserted by AIP] and shows how the clusters are mobile, i.e. the movie shows that this is a cluster fluid phase and not a cluster glass).

Figure 8a shows the variation of the equilibrium (configurational) energy with the number of large clusters. A minimum is observed in the region between 10 - 15 clusters. Figure 8b shows a snapshot of an equilibrium configuration from the simulation with 13 clusters. Therefore, MC simulations indicate that the most favorable cluster density is between $1.9\text{x}10^{-5}$ and $2.8\text{x}10^{-5}$ with clusters of 1065 to 710 particles respectively. This is in reasonable agreement with the thermodynamic model that predicts a cluster density of $1.5\text{x}10^{-5}$, with an average size of 1112 particles.

5. Summary

The thermodynamic model developed here for the cluster fluid phase of the SALR fluid is essentially a kind of micelle theory. However, it has some novel features that, to our knowledge, are unique in theories of micellization, and these lead to unique predictions. First, it is designed to operate on a pair potential $\phi(r)$ (i.e. it can predict how changes in phase behaviour depend on details of the pair potential). This approach is unusual, in that micelle theories are usually framed in terms of emergent properties, such as the binding energy per particle and interfacial tension which are often adjusted to reproduce experimental data. Second, the model is parameterized by four densities, and in this regard it can also be considered a kind of non-mean-field density functional theory. By including the liquid, or body, density in this set we are able, for the first time, to investigate how the cluster density is traded against the other parameters at equilibrium. In particular, this enables identification of a threshold beyond which clusters are likely to be solid particles, rather than liquid-like droplets. This, in turn, leads to our proposal for a non-classical two-step crystal nucleation process, similar to those proposed by others in earlier work based on a division of timescales between cluster formation and nucleation within clusters. The novel contribution of this work to the two-step proposal concerns the insight generated by the approximate cluster size formula, equation (43), which indicates that cluster size will change upon crystallization of the droplets. It will be interesting to investigate this proposal in future work, and in particular to discover if macroscopic crystals can grow out of microscopic droplets. Thirdly, the model is unique among theories of micellization for the SALR fluid in that $f_{mix}^{ex}(\rho_v, \rho_c) \neq 0$. This enables prediction of a novel cluster vapour to cluster liquid transition which we aim to investigate further by simulation of suitable equilibrium SALR systems in future work.

The phase behaviour predicted here might also be investigated by experimental means if suitable equilibrium SALR systems can be devised. The colloid-polymer systems used recently by Bartlett and co-workers[32,33] for which $\zeta \sim 1$ are interesting in this respect. It is not clear if these predictions can be confirmed by other kinds of experimental systems. Systems that might exhibit effective interactions similar to the SALR model will be those with relatively strong short ranged interactions, perhaps caused by hydrogen bonding, and weaker long ranged interactions, perhaps caused by charge dissociation in solution (i.e. by de-protonation or dissolution of other ionic groups). The list of systems that display these kinds of phenomena (e.g. hydrogen bonding and de-protonation in solution) is very long and encompasses solutions of amines, amino acids, peptides, and many other molecules of biological relevance. For example, clusters have recently been observed experimentally in aqueous glycine solutions[30]. However, there is considerable debate about the existence and cause of clusters like these in molecular liquid mixtures. It is frequently argued that they could be caused

by impurities, and due to the length-scales involved it is difficult to refute this. Nevertheless, clustering in these molecular liquids could be in the equilibrium regime due to the length and energy-scales involved, and it would be interesting if this could be confirmed.

The thermodynamic model developed here is most appropriate for large clusters where the influence of interfacial entropy and roughness, which the model neglects, are less significant. We have applied it to one particular combination of SALR parameters where large clusters are expected. We expect the behaviour obtained for this particular set is quite general, but nevertheless it will be interesting to map equilibrium cluster fluid behaviour for a much wider range of parameters. In particular, it will be interesting to apply the model to smaller values of ζ where non-equilibrium effects are more likely in simulations and experiment. In cases where such frustrated phases occur the model might reveal the underlying equilibrium phase towards which these phases are slowly evolving, which could be one of the cluster phases described here.

We are now in a position to comment on previous work by Bomont et al.[45] based on self-consistent integral equation methods. They find evidence of long-ranged correlations that grow quickly with small changes of system parameters, suggestive of clustering, and observe a jump in structural properties over a narrow range of system parameters. Their results are obtained for a two-Yukawa fluid similar to ours, but with slightly different parameters (A_r/A_a = 0.1, z_a = 1.5, and z_r = 0.5; with 0.86 <A_a< 0.91) and at much higher densities than we investigate here, ρ_b = 0.382. At these high densities, our work indicates that the cluster fluid will not be seen, since instead modulated phases are expected. However, Figure 2 does indicate the possibility of a first order transition from the bulk vapour (with pre-clusters) to a modulated phase at sufficiently high densities and low values of A_a. We suggest the jump they observe in structural properties might correspond to this transition.

References

[1] A. Stradner, H. Sedgwick, F. Cardinaux, W. C. K. Poon, S. U. Egelhaaf, and P. Schurtenbuerger, *Nature* **432**, 492 (2004).

[2] J. Chen, B. Sarma, J. M. B. Evans, and A. S. Myerson, *J. Crystal Growth & Design* **11**, 887 (2011).

[3] D. Gebauer, A. Völkel and H. Cölfen H, *Science* **322**, 1819 (2008).

[4] M. Li, H. Schnablegger and S. Mann, *Nature* **402**, 393 (1999).

[5] X. Zhang, H. Sun and S. Yang, *J. Phys. Chem. C* **116**, 19018 (2012).

[6] H. Cölfen and S. Mann, *Angewandte Chemie* **42**, 2350 (2003).

[7] Y. M. Ramdzan, S. Polling, C. P. Z. Chia, I. H. W. Ng, A. R. Ormsby, N. P. Croft, A. W. Purcell, M. A. Bogoyevitch, D. C. H. Ng, P. A. Gleeson, and D. M. Hatters, *Nature Methods* **9**, 467 (2012).

[8] R. Varma and S. Mayor, *Nature* **394**, 798-801 (1998).

[9] D. Lingwood and K. Simons, *Science* **327**, 46-50 (2010).

[10] N. Meilhac and N. Destainville, *J. Phys. Chem. B* **115**, 7190 (2011).

[11] A. R. Hirst, S. Roy, M. Arora, A. K. Das, N. Hodson, P. Murray, S. Marshall, N. Javid, J. Sefcik, J. Boekhoven, J. H. van Esch, S. Santabarbara, N. T. Hunt, and R. V. Ulijn, *Nature Chemistry* **2**, 1089 (2010).

[12] M.M. Stevens, N. T. Flynn, C. Wang, D. A. Tirrell, and R. Langer, *Advanced Materials* **16**, 915 (2004).

[13] F. Sciortino, S. Mossa, E. Zaccarelli, and P. Tartaglia, *Phys. Rev. Lett.* **93**, 055701 (2004).

[14] F. Cardinaux, A. Stradner, P. Schurtenberger, F. Sciortino, and E. Zaccarelli, *Europhys. Lett.* **77**, 48004 (2007).

[15] P. Kowalczyk, A. Ciach, P. A. Gauden, and A. P. Terzyk, *J. Colloid & Interface Sci.* **363**, 579 (2011).

[16] F. Cardinaux, E. Zaccarelli, A. Stradner, S. Bucciarelli, B. Farago, S. U. Egelhaaf, F. Sciortino, and P. Schurtenberger, *J. Phys. Chem.* B **115**, 7227–7237 (2011).

[17] A. Campbell, V. J. Anderson, J. S. van Duijneveldt, and P. Bartlett, *Phys. Rev. Lett* **94**, 208301 (2005).

[18] C. J. Dibble, M. Kogan, and M. J. Solomon, *Phys. Rev. E* **74**, 041403 (2006).

[19] M. M. van Schooneveld, V. W. A. de Villeneuve, R. P. A. Dullens, D. G. A. L. Aarts, M. E. Leunissen, and W. K. Kegel, *J. Phys. Chem. B* **113**, 4560 (2009).

[20] J. M. Bomont, J. L. Bretonnet, and D. Costa, *J. Chem. Phys.* **132**, 184508 (2010).

[21] C. L. Klix, C. P. Royall, and H. Tanaka, *Phys. Rev. Lett.* **104**, 165702 (2010).

[22] Y. Liu, L. Porcar, J. Chen, W. R. Chen, P. Falus, A. Faraone, E. Fratini, O. K.Hong, and P. Baglioni, *J. Phys. Chem. B* **115**, 7238 (2011).

[23] G. Foffi, C. De Michele, F. Sciortino, and P. Tartaglia, *J. Chem. Phys.* **122**, 224903 (2005).

[24] P.R. ten Wolde and D. Frenkel, Science 277, 1975 (1997).

[25] R. P. Sear, *J. Chem. Phys.* **131**, 074702 (2009).

[26] P. G. Vekilov, *J. Crystal Growth & Design* **10**, 5007 (2010).

[27] D. Erdemir, A. Y. Lee, and A. S. Myerson, *Acc. Chem. Res.* **42,** 621 (2009).

[28] O. Galkin, W. C. Pan, L. Filobelo, R. E. Hirsch, R. L. Nagel, and P. G. Vekilov, *Biophys. J.* **93**, 902 (2007).

[29] V. Uzunova, W. C. Pan, V. Lubchenko, and P. G. Vekilov, J. Chem. Soc., *Faraday Discussions* **159**, 87 (2012).

[30] A. Jawor-Baczynska, J. Sefcik, and B. D. Moore, *Crystal Growth & Design* **13**, 470 (2013).

[31] M. Kellermeier, R. Rosenberg, A. Moise,U. Anders, M. Przybylski, and H. Cölfen, *J. Chem. Soc., Faraday Discussions* **159**, 23 (2012).

[32] L. J. Teece, M. A. Faers, and P. Bartlett, *Soft Matter* **7**, 1341-1351 (2011).

[33] I. Zhang, C. P. Royall, M. A. Faers, and P. Bartlett, *Soft Matter* **9**, 2076 (2013).

[34] A. J. Archer and N. B. Wilding, *Phys. Rev. E* **76**, 031501 (2007).

[35] A. J. Archer, *Phys. Rev. E* **78**, 031402 (2008).

[36] D. F. Schwanzer and G. Kahl, *J. Phys.: Condens. Matter* **22**, 415103 (2010).

[37] A. J. Archer, C. Ionescu, D. Pini, and L. Reatto, *J. Phys.: Condens. Matter* **20**, 415105 (2008).

[38] A. Ciach, Phys. Rev. E **78**, 061505 (2008).

[39] A. Ciach and W. T. Gozdz, *Condens. Matter Phys.* **13**, 23603 (2010).

[40] A. J. Archer, D. Pini, R. Evans, and L. Reatto, *J. Chem. Phys.* **126**, 014104 (2007).

[41] J. M. Bomont and D. Costa, *J. Chem. Phys.* **137**, 164901 (2012).

[42] T. H. Zhang, J. Klok, R. H. Tromp, J. Groenewold, and W. K. Kegel, *Soft Matter* **8**, 667-672 (2012).

[43] T. Jiang and J. Z. Wu, *Phys. Rev. E* **80**, 021401, (2009).

[44] F. H. Stillinger, *J. Chem. Phys.* **78**, 4654 (1983).

[45] J. M. Bomont, J. L. Bretonnet, D. Costa, and J. P. Hansen, *J. Chem. Phys.* **137**, 011101 (2012).

[46] J. M. Kim, R. Castaneda-Priego, Y. Liu, and N. J. Wagner, *J. Chem. Phys*. **134**, 064904 (2011).

[47] C. Tanford, J. Phys. Chem.**78**, 2469 (1974).

[48] R. Nagarajan and E. Ruckenstein*, J. Colloid & Interface Sci.* **60**, 221 (1977).

[49] D. J. Mitchell and B. W. Ninham, *J. Chem. Soc.: Faraday Trans. 2* **77**, 601 (1981).

[50] S. Puvvada and D. Blankschtein, *J. Chem. Phys.* **92**, 3710 (1990).

[51] L. Maibaum, A. R. Dinner, and D. Chandler, *J.Phys. Chem. B* **108**, 6778 (2004).

[52] J. Groenewold and W. K. Kegel, *J. Phys.: Condens. Matter* **16**, S4877 (2004).

[53] N. Destainville and L. Foret, *Phys. Rev. E* **77** 051403 (2008).

[54] M. B. Sweatman and N. Quirke, *J. Phys. Chem. B* **109**, 10381 (2005).

[55] M. B. Sweatman and N. Quirke, *J. Phys. Chem. B* **109**, 10389 (2005).

[56] J. P. Hansen and I. R. McDonald, *Theory of Simple Liquids*, Academic Press, 2nd Edition (1986).

[57] Y. Rosenfeld, *Phys. Rev. Lett*. **63**, 980 (1989).

[58] D. Frenkel and B. Smit, *Understanding Molecular Simulation: From Algorithms to Applications, (*Academic, New York, 1996).

[59] See Supplementary Material Document No._____ for a movie showing the fluid-like nature of the droplets.

Figures

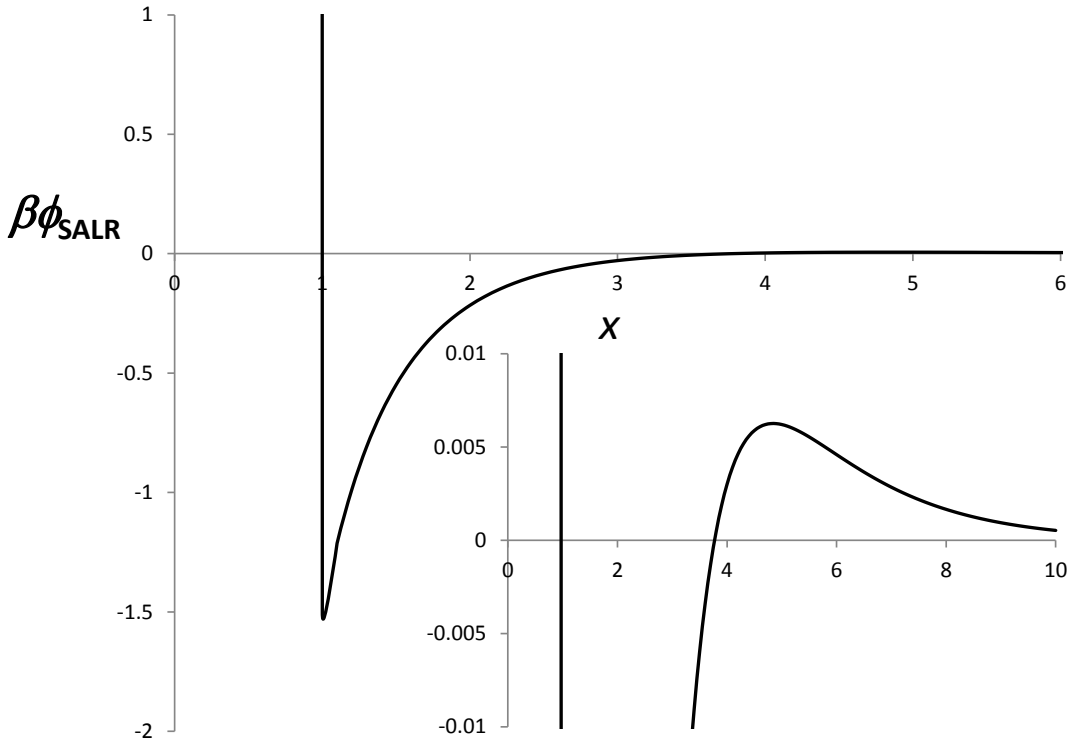

Figure 1a. The SALR potential investigated in this work, with A_a = 2.0, A_r = 0.5, z_a = 1.0, and z_r = 0.5. The inset shows the long range repulsive contribution on a larger scale.

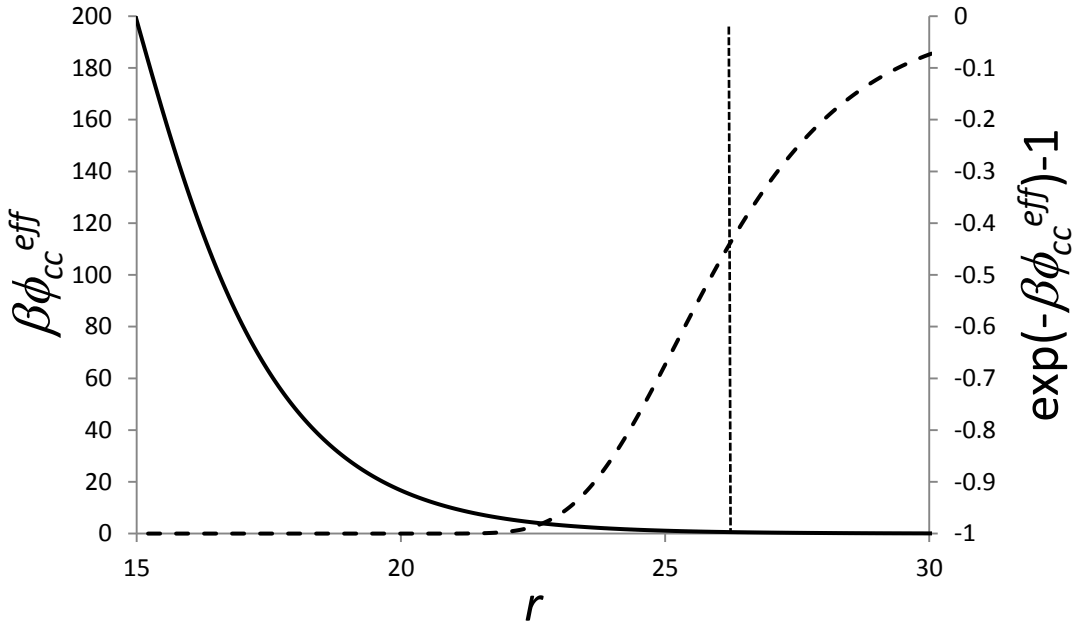

Figure 1b. Effective cluster-cluster interaction (full line) for the same system as Figure 1a, with bulk density ρ_b = 0.01, corresponding to equilibrium cluster diameter d_c = 13.49d. The corresponding Mayer-f function (dotted line) is shown on the right-hand axis, along with the effective cluster-cluster hard sphere diameter (d_c^{eff} = 26.30d) determined via the Barker-Henderson route (equation (17)) shown as the dashed vertical line.

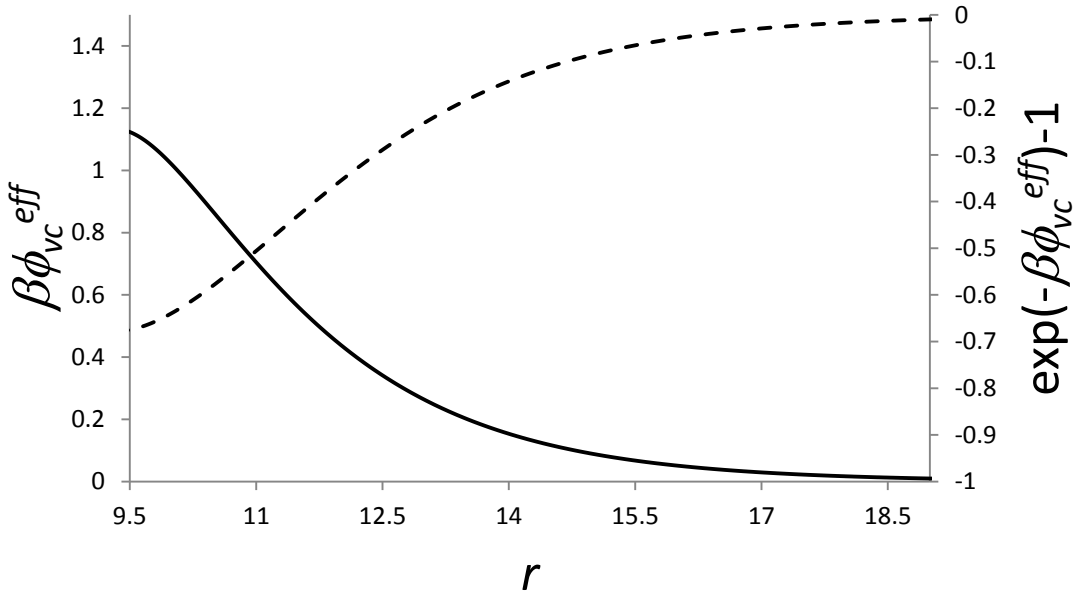

Figure 1c. Effective particle-cluster interaction (full line) for the same system as in Figure 1b.The corresponding Mayer-f function (dotted line) is shown on the right-hand axis.

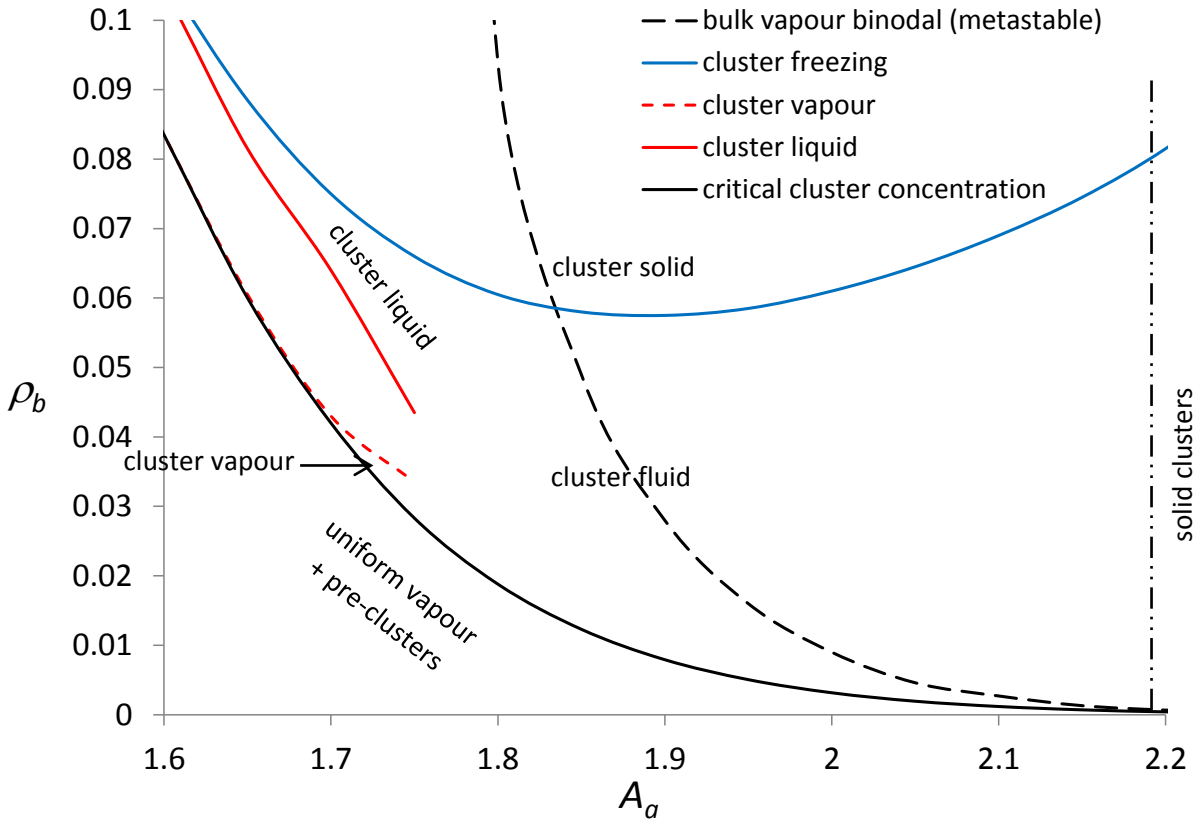

Figure 2. Low density phase diagram of the cluster fluid for the SALR parameters A_r = 0.5, z_a = 1.0, z_r = 0.5, and a range of values for A_a. The full black line is the critical cluster concentration (CCC) that denotes the boundary of the cluster fluid phase. The cluster fluid phase occurs at densities higher then CCC, while for densities less than the CCC the bulk vapour exhibits pre-clusters. The long-dashed black line is the metastable vapour branch of the bulk vapour-liquid transition. The blue line signifies our estimate for a phase transition from the cluster fluid to an ordered, or modulated, phase, possibly a cluster 'solid'. The red lines signify a first-order cluster vapour to cluster liquid transition. At around A_a = 1.65 the cluster vapour becomes unstable with respect to the bulk vapour containing pre-clusters, producing a bulk vapour (with pre-clusters) to cluster liquid transition. We expect the cluster fluid – cluster liquid transition terminates at a critical point close to A_a = 1.75.The dashed-dot-dot line at A_a = 2.19 indicates that solid particle clusters are expected above this value.

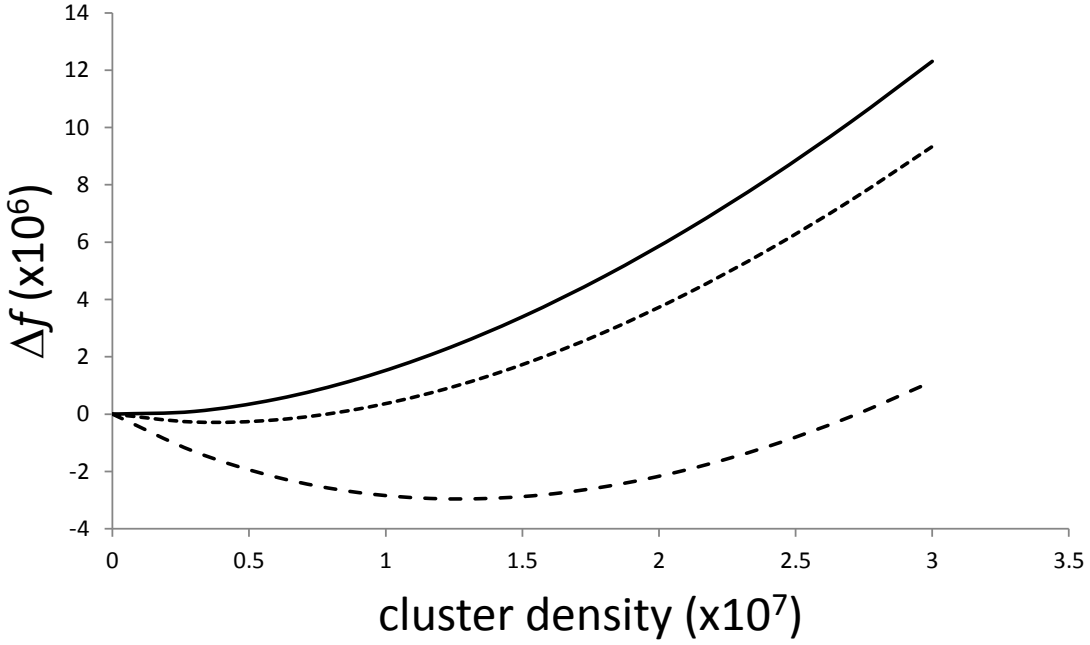

Figure 3a. Difference, Δf, in the free energy density of the cluster fluid phase and the uniform bulk phase at the same bulk density for the SALR parameters A_a = 2.0, A_r = 0.5, z_a = 1.0, and z_r = 0.5 and for a range of cluster densities and three bulk densities; ρ_b = 0.00315 (very slightly below the CCC, full line), ρ_b = 0.0032 (slightly above the CCC, short-dashed line), and ρ_b = 0.0033 (somewhat above the CCC, long-dashed line).

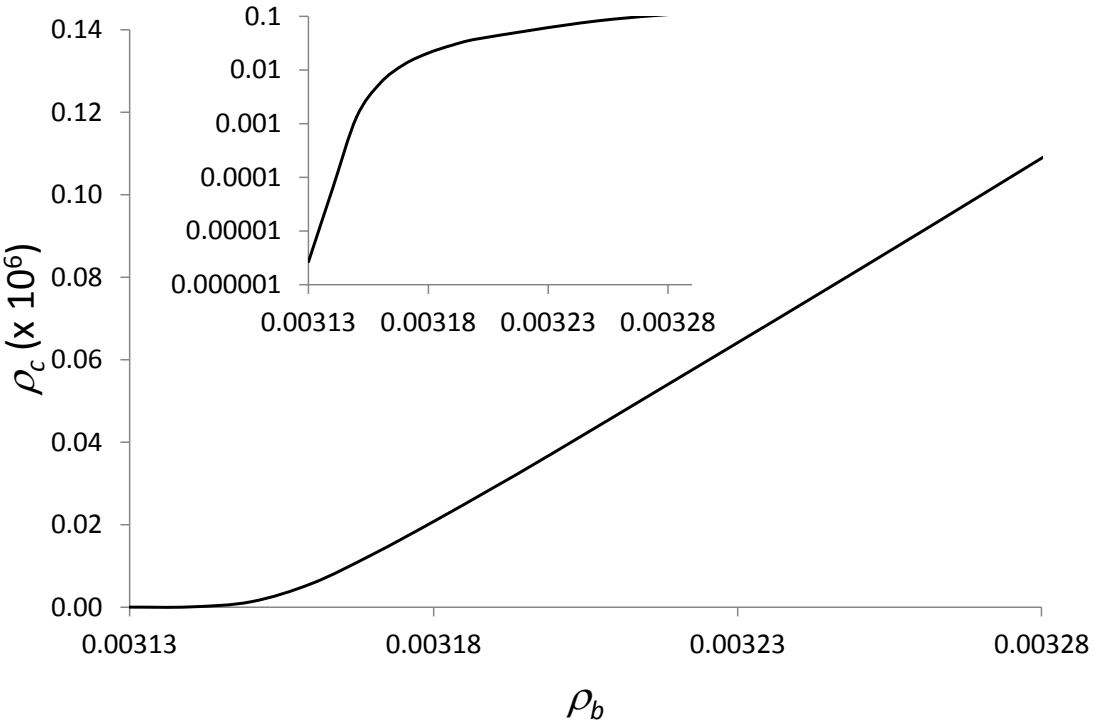

Figure 3b.Variation of cluster density with bulk density for the same SALR parameters as in Figure 3a. The trend is nearly linear above the CCC (0.003155), while the inset shows it is nearly exponential below the CCC.

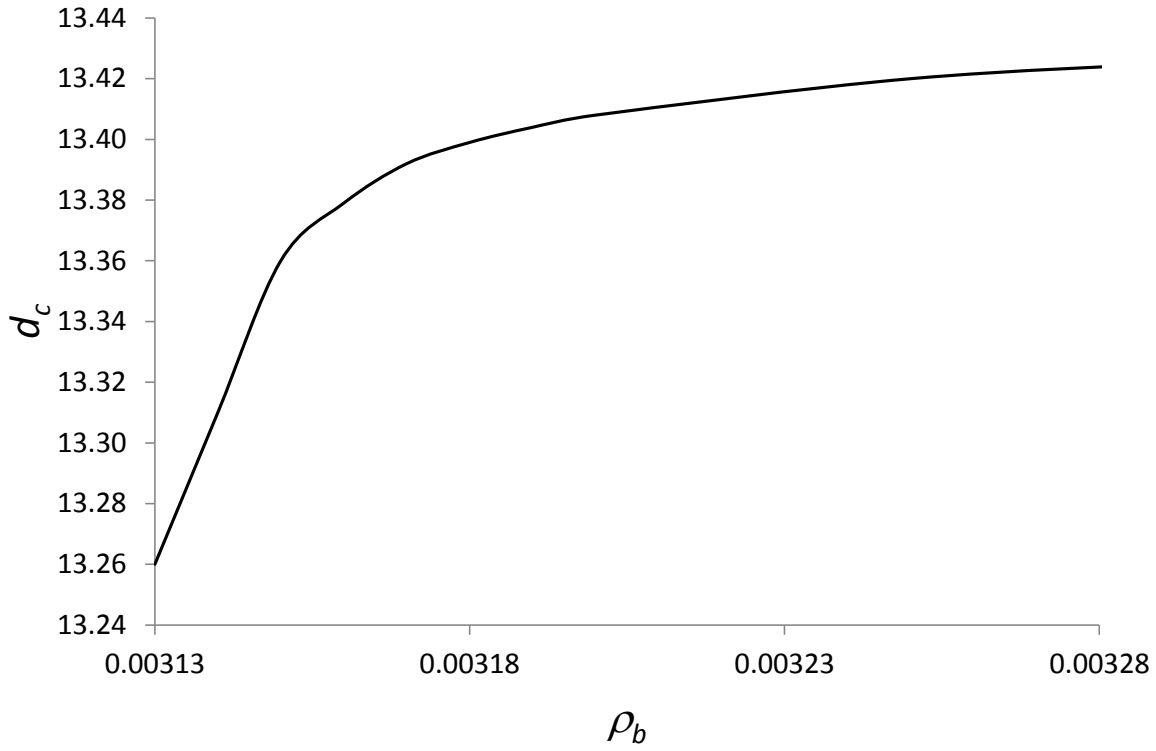

Figure 3c.Variation of cluster diameter with bulk density for the same SALR parameters as in Figure 3a. A 'knee' is clearly observed in the vicinity of the CCC.

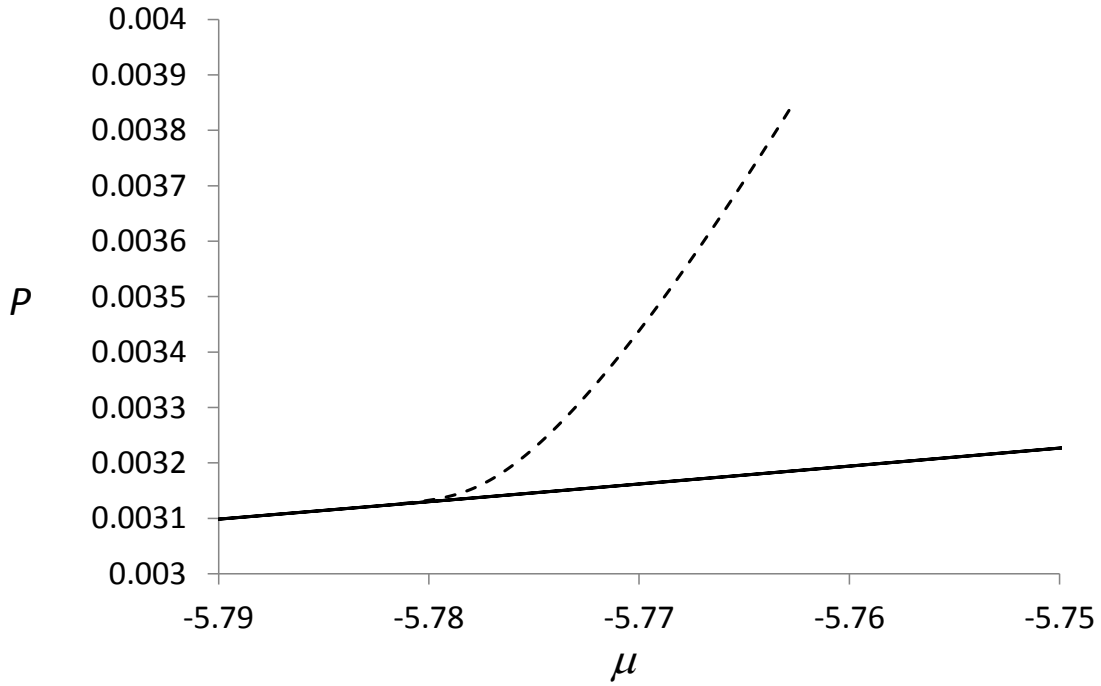

Figure 3d. Pressure, *P*, is plotted for a range of chemical potentials, μ, for the same system as Figure 3a. At low chemical potential the uniform vapour phase without clusters (solid line) is indistinguishable from the pre-cluster/cluster fluid branch on the scale of this plot. At μ = -5.78, corresponding to ρ_b = 0.006 and prior to the bulk vapour-liquid transition at ρ_b = 0.0089, the cluster fluid phase branch (dashed line) clearly separates from the uniform vapour branch, which is always metastable. The cluster fluid phase pressure increases slowly with bulk density, and we expect a transition to a modulated cluster 'solid' phase occurs close to μ = -5.763, corresponding to ρ_b = 0.061.

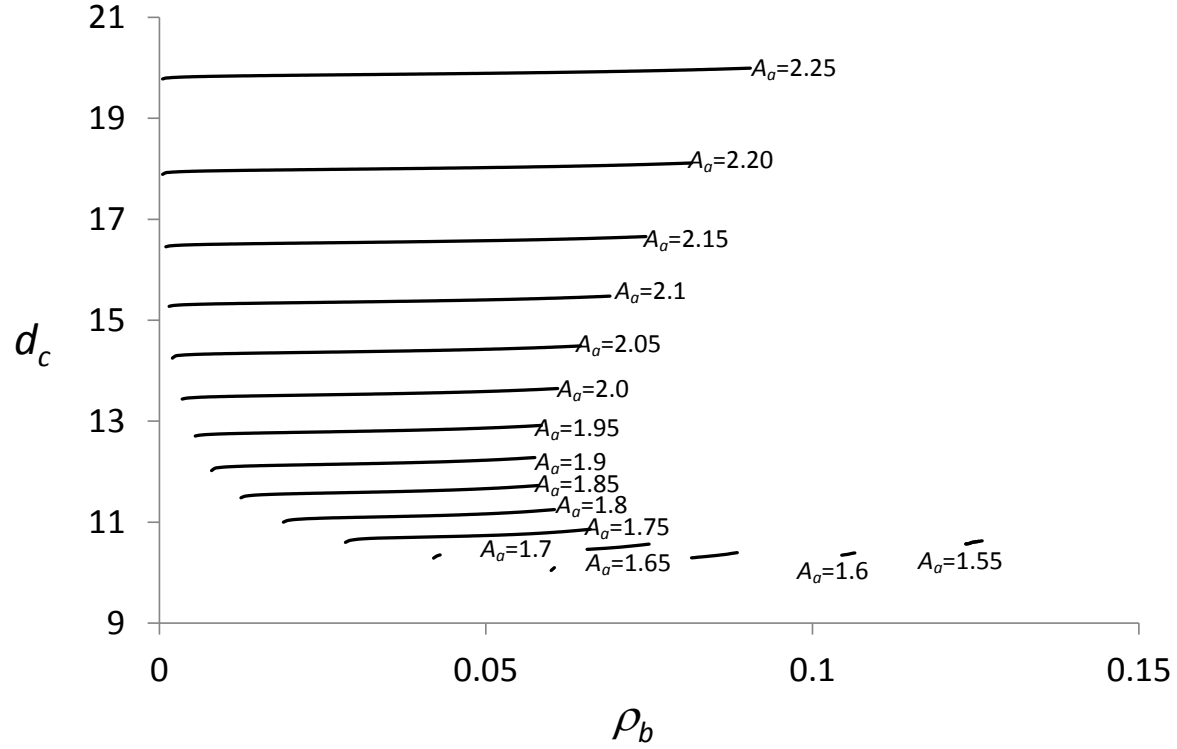

Figure 4a.Variation of cluster diameter with A_a and bulk density for the same system as Figure 2.

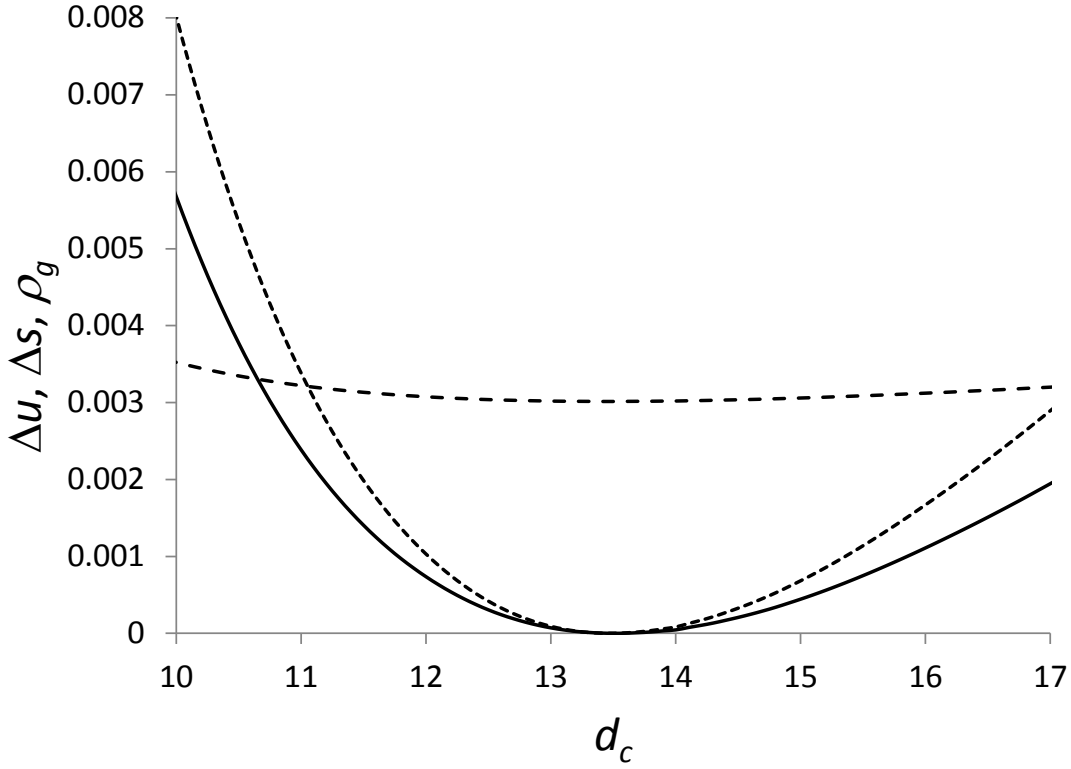

Figure 4b. Variation of i) the difference in the configurational entropy density from its minimum value (Δs, full line), ii) the difference in the configurational energy density from its minimum value(Δu, short-dashed line), and iii) the vapour density (ρ_g, long-dashed line), with cluster size for the same SALR system as Figure 3awith ρ_b = 0.02. The energy minimum coincides with an entropy minimum and a minimum in the vapour density.

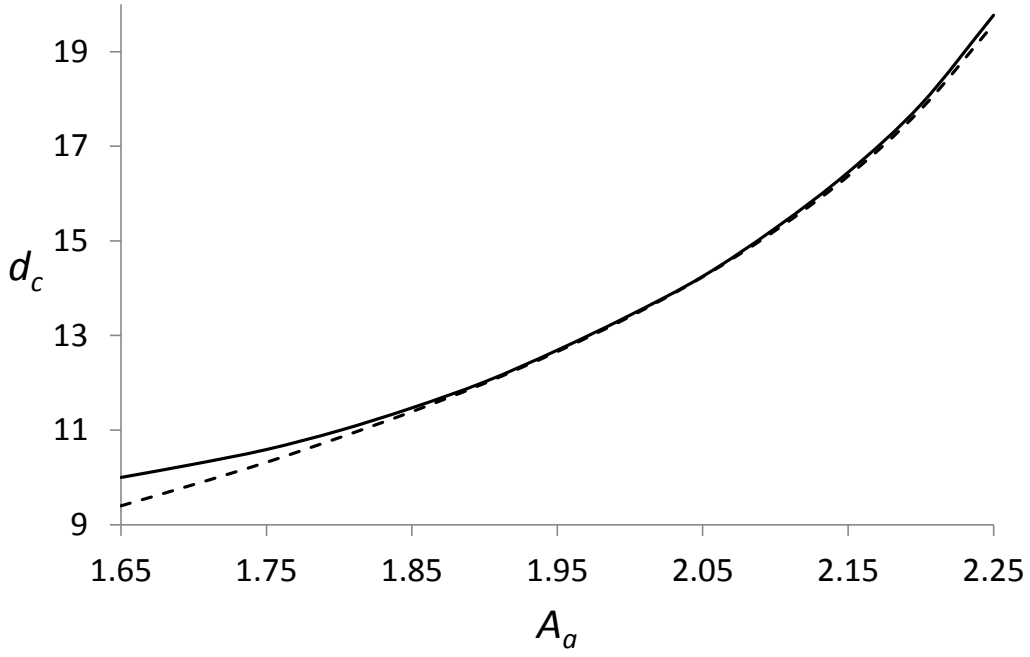

Figure 4c. Comparison of cluster size along the CCC predicted via the full model (minimisation of equation (29), dashed line) and via equation (43) with ρ_l = 086 (solid line). The SALR parameters are the same as for Figure 2.

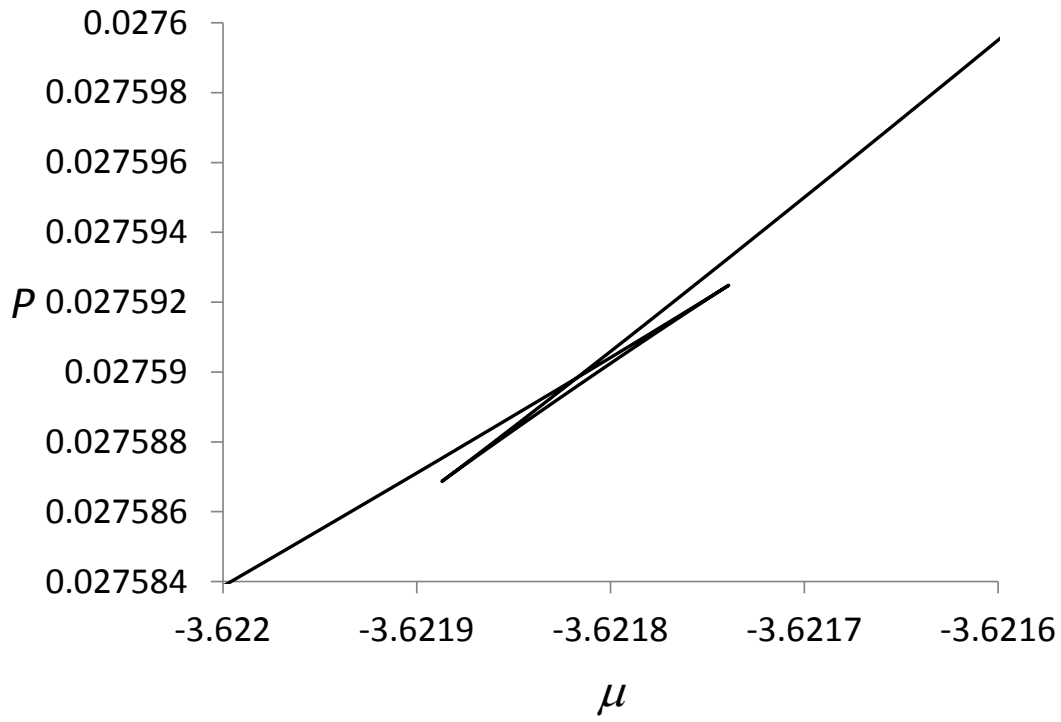

Figure 5.Variation of pressure with chemical potential for the SALR parameters A_a = 1.75, A_r = 0.5, z_a = 1.0, and z_r = 0.5showing the intersection of the cluster fluid phase signifying a first-order cluster vapour to cluster liquid transition at μ = -3.62182 and P = 0.02759.

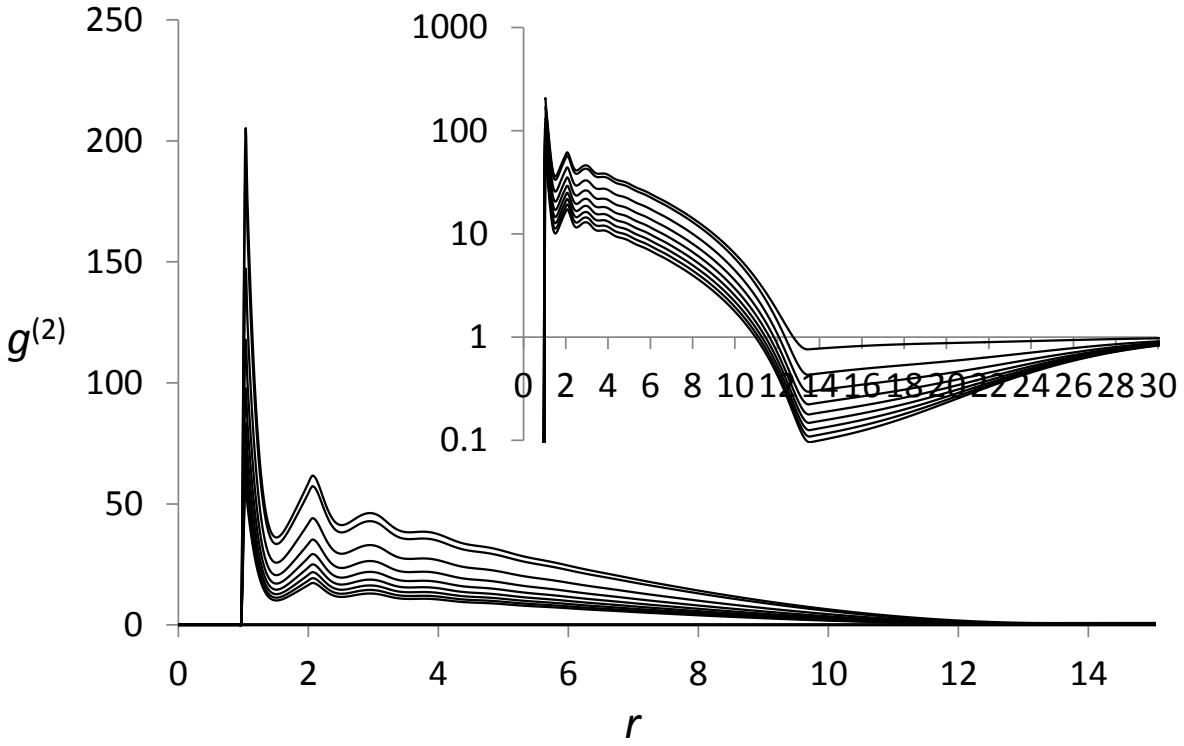

Figure 6.Radial distribution function generated by equations (8) and (11)for the SALR parameters A_a = 2.0, A_r= 0.5, z_a = 2.0, and z_r = 1.0 for a series (starting at the top)of bulk densities above the CCC, ρ_b = 0.005, 0.01, 0.015, 0.02, 0.025, 0.03, 0.035, 0.04, 0.045, and 0.05. The inset is on a logarithmic scale.

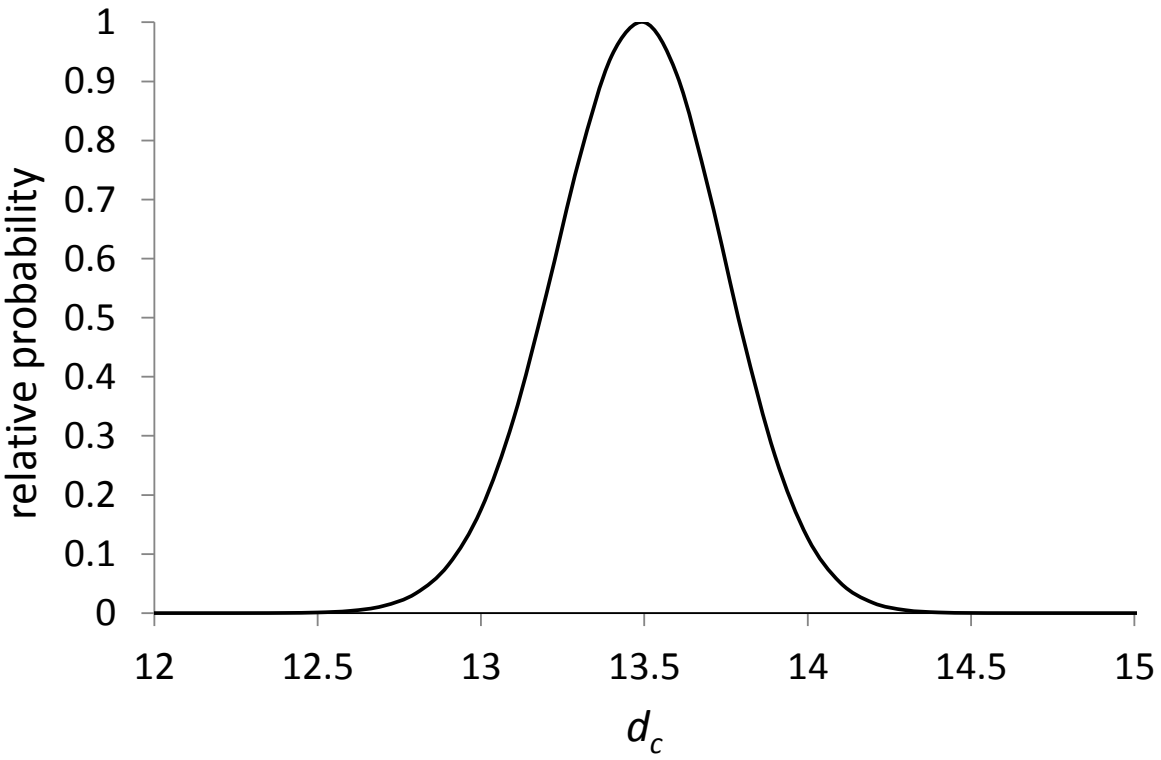

Figure 7.Estimate, using equation (46) and the procedure outlined in the text, of the relative probability distribution for cluster size fluctuations for the same SALR system as Figure 6 at ρ_b = 0.01.

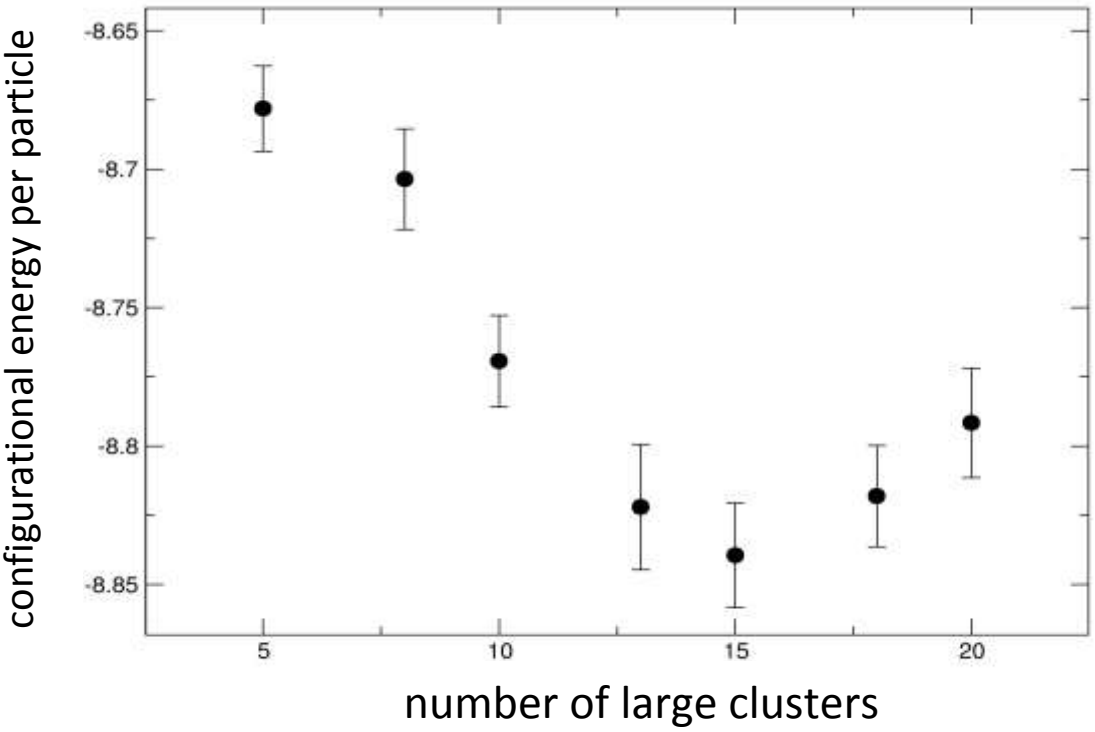

Figure 8a: Average configurational energy per particle at equilibrium for Monte Carlo simulations with different numbers of large clusters. System details: number of particles = 10648, system volume = 532400 (ρ_b=0.02), SALR parameters: A_a = 2.0, A_r= 0.5, z_a = 1.0, and z_r = 0.5. Standard errors are provided at the level of two standard deviations.

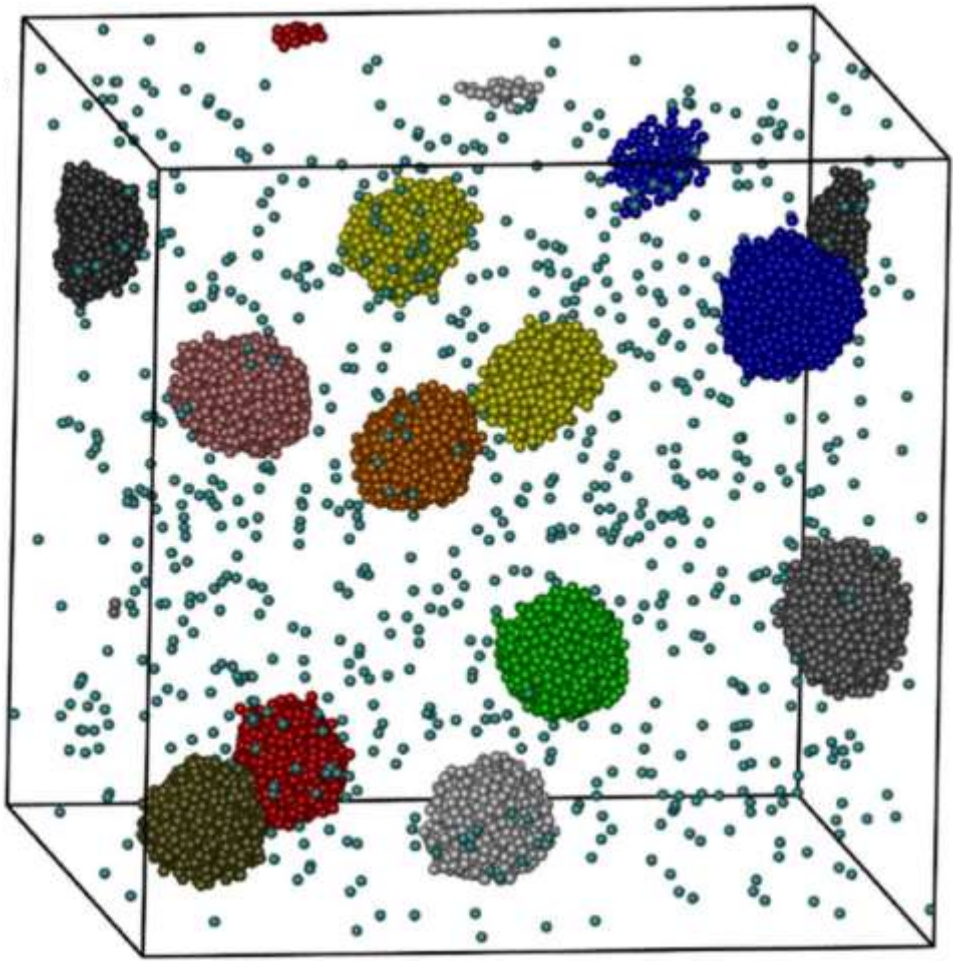

Figure 8b. Snapshot of an equilibrium configuration from a system with 13 clusters, where the SALR parameters are the same as those used in Figure 8a. Colouring is used to differentiate clusters and the background vapour.

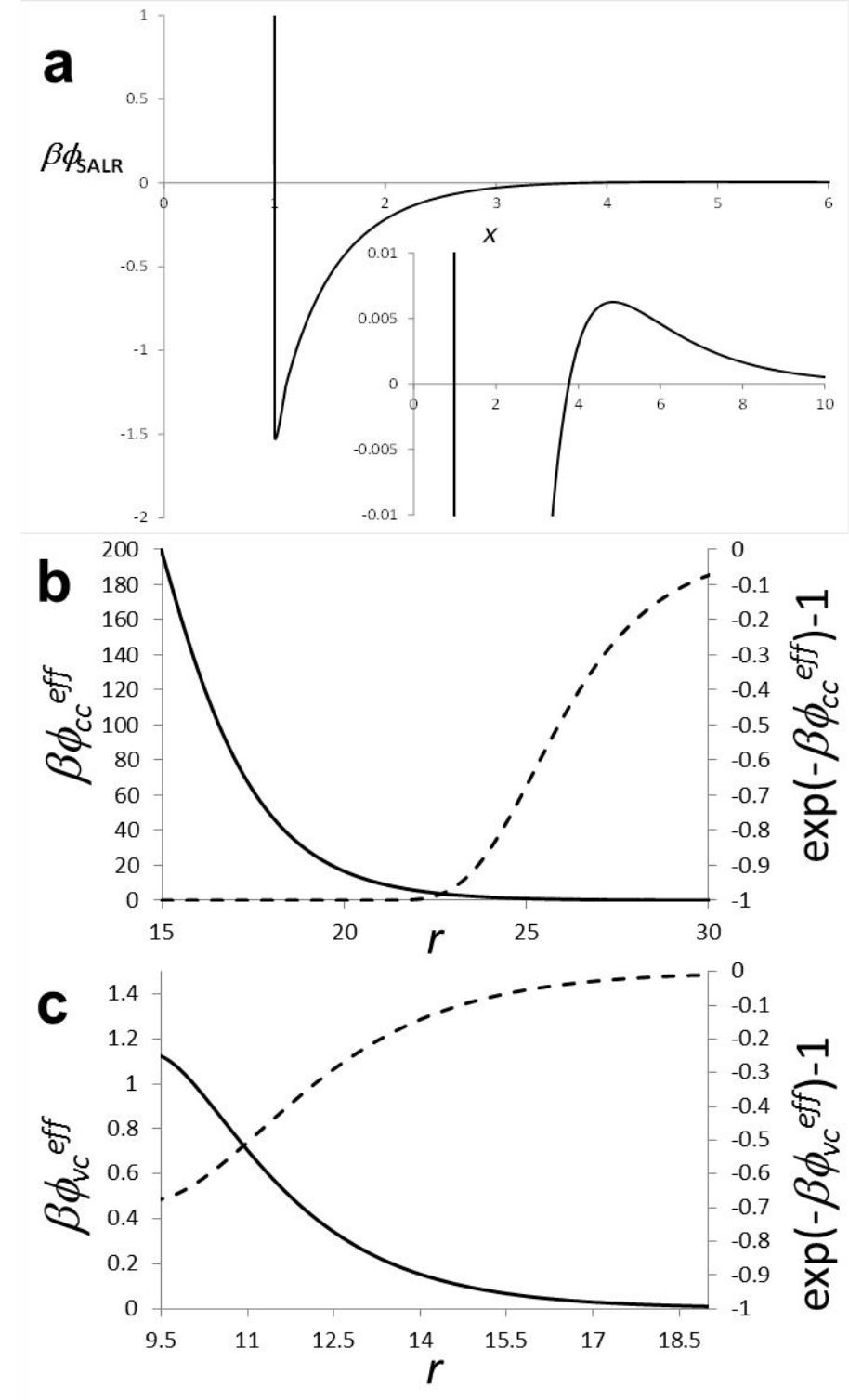
a
$\beta\phi_{SALR}$
x
b
$\beta\phi_{cc}^{eff}$
$\exp(-\beta\phi_{cc}^{eff})-1$
r
c
$\beta\phi_{vc}^{eff}$
$\exp(-\beta\phi_{vc}^{eff})-1$
r

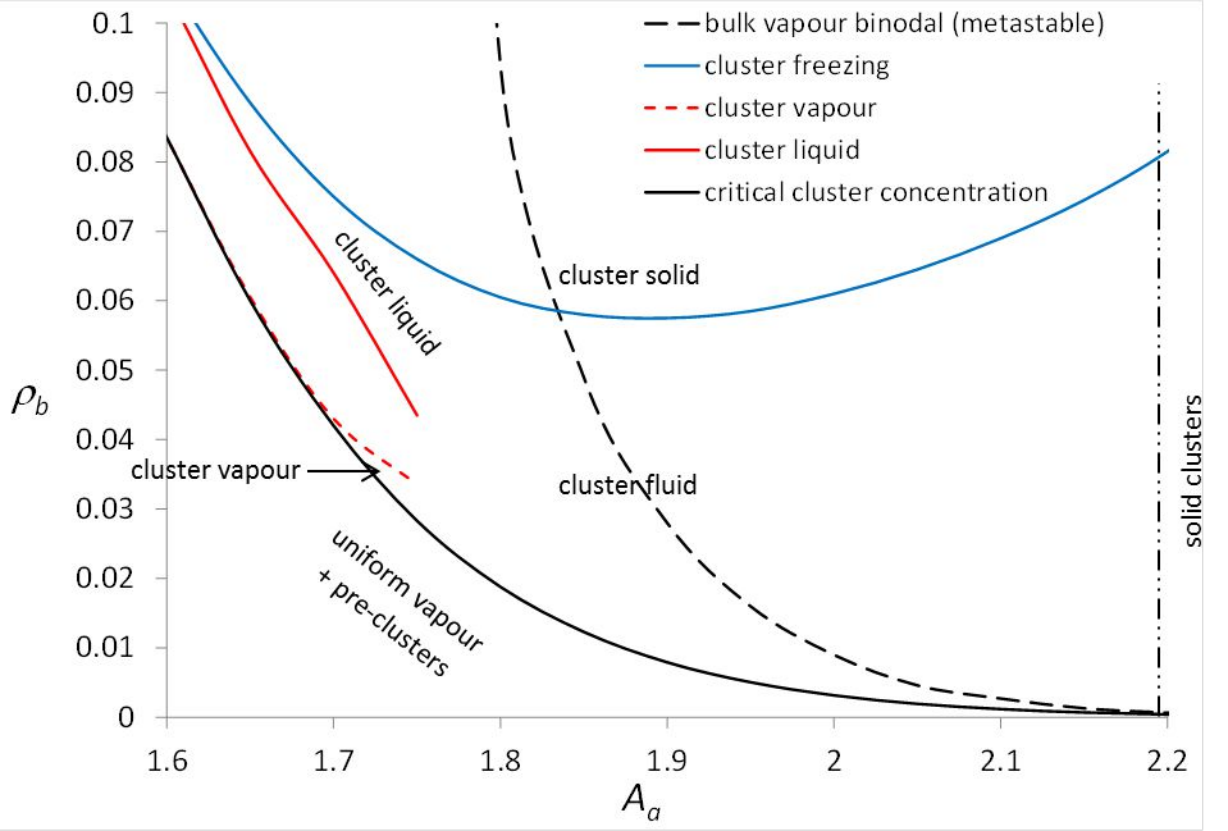
bulk vapour binodal (metastable)
cluster freezing
cluster vapour
cluster liquid
critical cluster concentration
cluster solid
cluster liquid
cluster vapour
cluster fluid
uniform vapour
+ pre-clusters
solid clusters
ρ_b
A_a
0.1
0.09
0.08
0.07
0.06
0.05
0.04
0.03
0.02
0.01
0
1.6
1.7
1.8
1.9
2
2.1
2.2

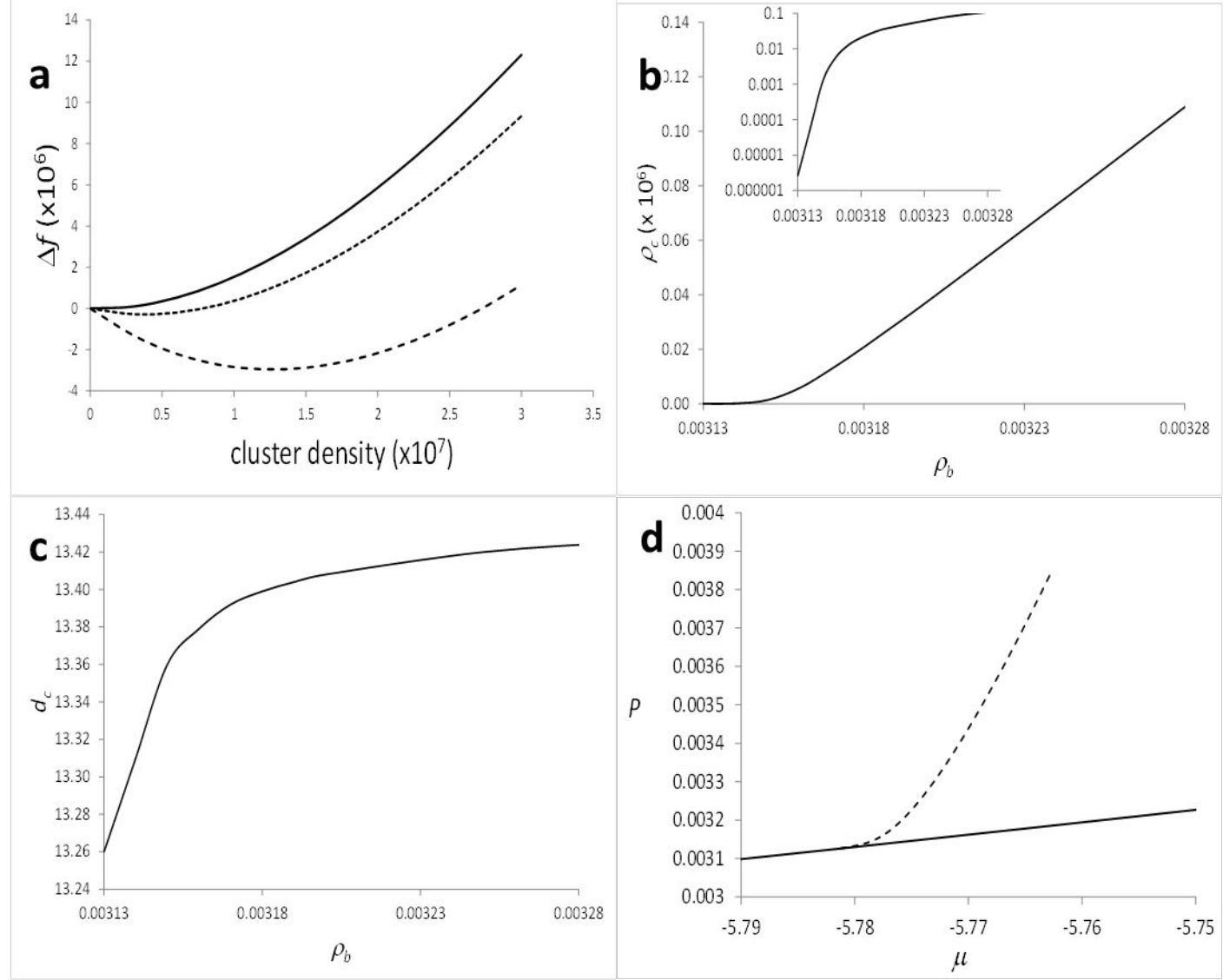
a
Δf (x10^6)
cluster density (x10^7)
b
ρ_c (x 10^6)
ρ_b
c
d_c
ρ_b
d
P
μ

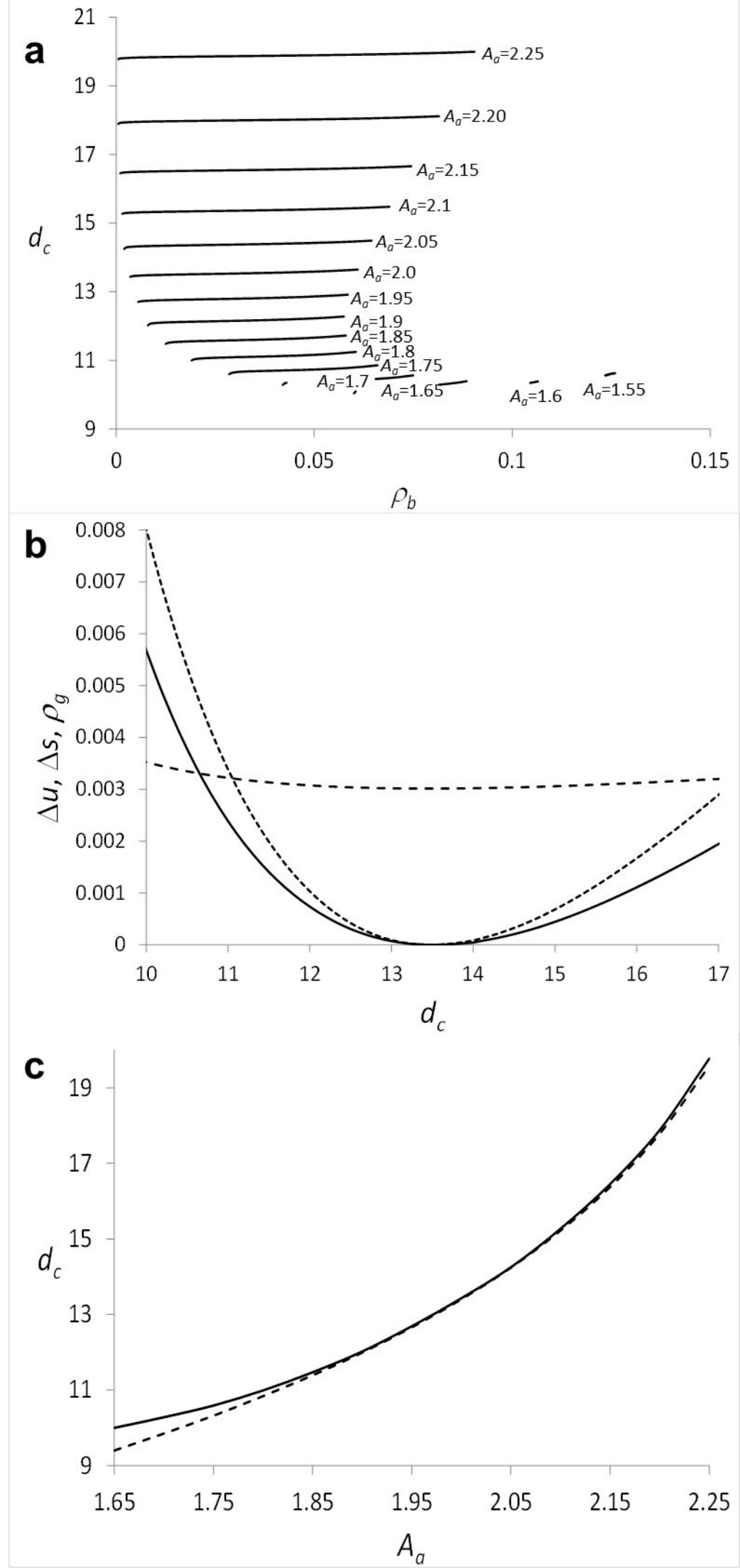
a
21
19
17
15
13
11
9
d_c
A_a=2.25
A_a=2.20
A_a=2.15
A_a=2.1
A_a=2.05
A_a=2.0
A_a=1.95
A_a=1.9
A_a=1.85
A_a=1.8
A_a=1.75
A_a=1.7
A_a=1.65
A_a=1.6
A_a=1.55
0
0.05
0.1
0.15
ρ_b
b
0.008
0.007
0.006
0.005
0.004
0.003
0.002
0.001
0
$\Delta u, \Delta s, \rho_g$
10
11
12
13
14
15
16
17
d_c
c
19
17
15
13
11
9
d_c
1.65
1.75
1.85
1.95
2.05
2.15
2.25
A_a

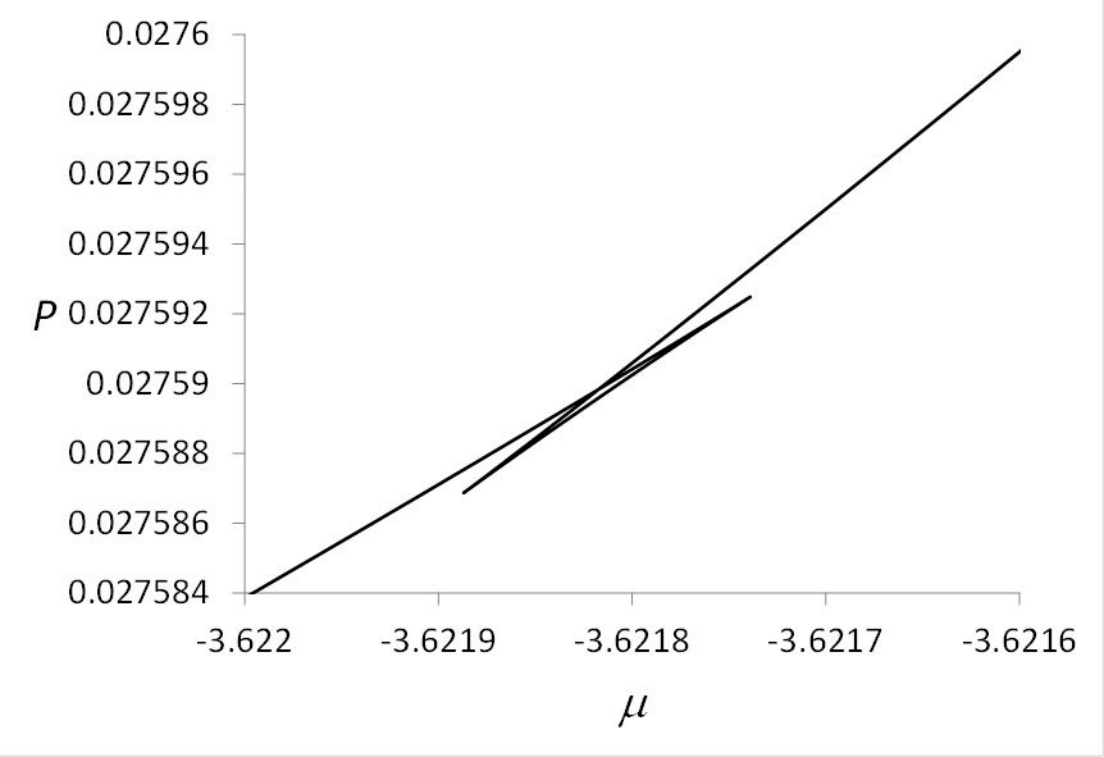
0.0276
0.027598
0.027596
0.027594
P 0.027592
0.02759
0.027588
0.027586
0.027584
-3.622
-3.6219
-3.6218
-3.6217
-3.6216
μ

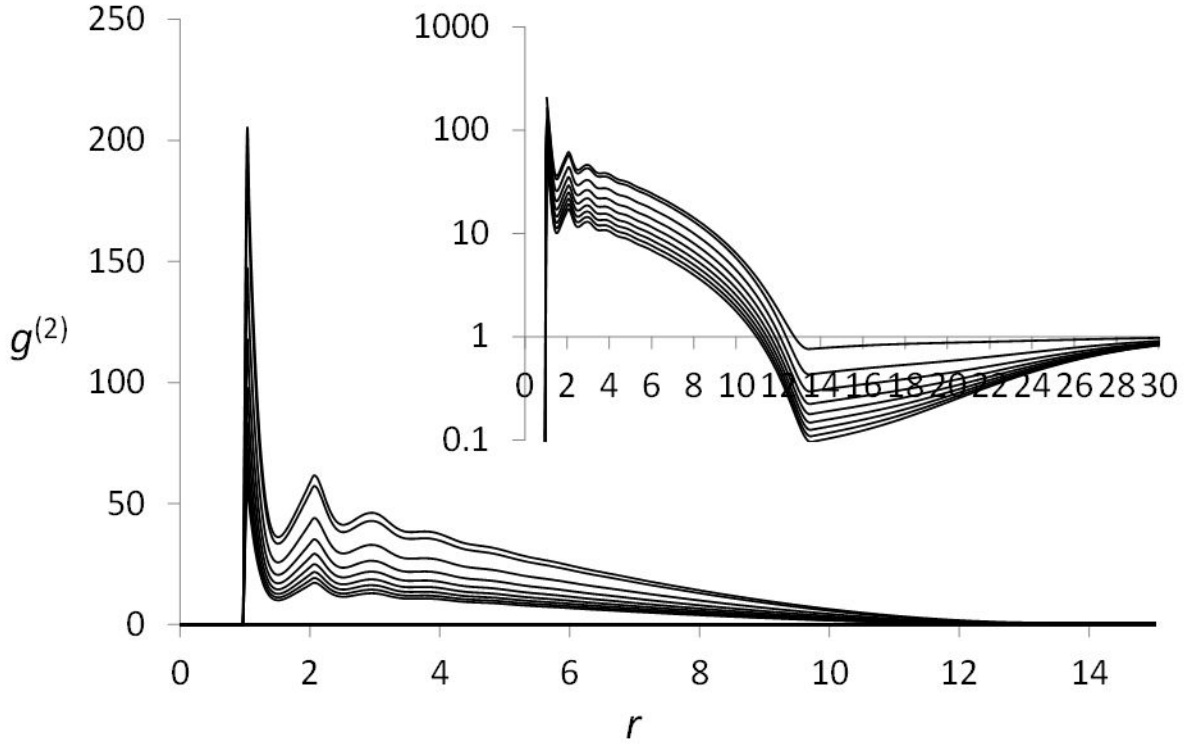
250
200
150
100
50
0
$g^{(2)}$
0
2
4
6
8
10
12
14
r
1000
100
10
1
0.1
0 2 4 6 8 10 12 14 16 18 20 22 24 26 28 30

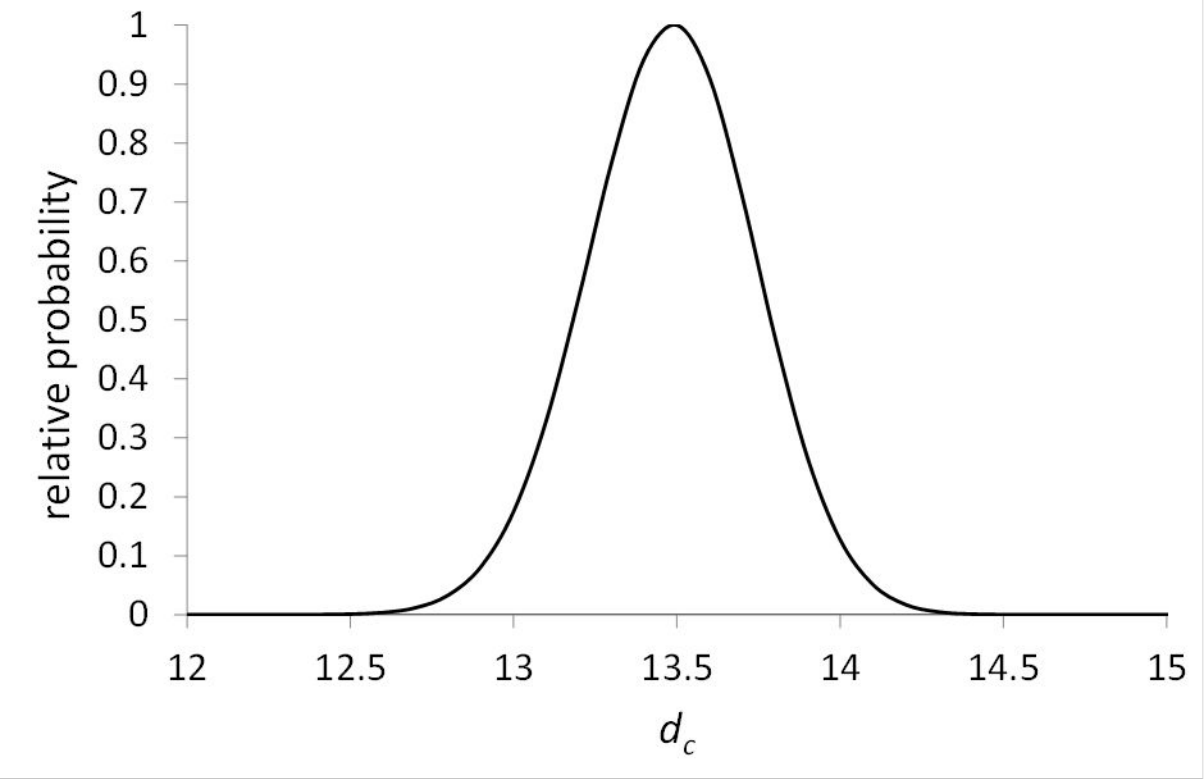
relative probability
1
0.9
0.8
0.7
0.6
0.5
0.4
0.3
0.2
0.1
0
12
12.5
13
13.5
14
14.5
15
d_c

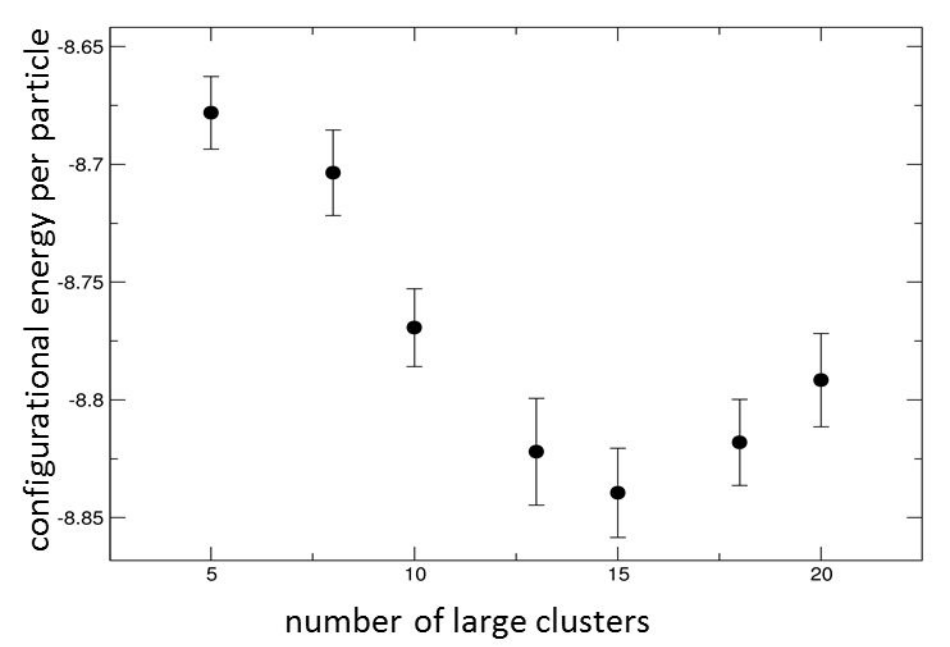
configurational energy per particle
-8.65
-8.7
-8.75
-8.8
-8.85
5
10
15
20
number of large clusters